

# Frequency Response Analysis for Reset Control Systems: Application to Predict Precision of Motion Systems

Xinxin Zhang<sup>a</sup>, Marcin B Kaczmarek<sup>a</sup>, S. Hassan HosseinNia<sup>a,\*</sup>

<sup>a</sup>Department of Precision and Microsystems Engineering (PME), Delft University of Technology, Mekelweg 2, Delft, 2628CD, The Netherlands

## Abstract

The frequency response analysis describes the steady-state responses of a system to sinusoidal inputs at different frequencies, providing control engineers with an effective tool for designing control systems in the frequency domain. However, conducting this analysis for closed-loop reset systems is challenging due to system nonlinearity. This paper addresses this challenge through two key contributions. First, it introduces novel analysis methods for both open-loop and closed-loop reset control systems at steady states. These methods decompose the frequency responses of reset systems into base-linear and nonlinear components. Second, building upon this analysis, the paper develops closed-loop higher-order sinusoidal-input describing functions for reset control systems at steady states. These functions facilitate the analysis of frequency-domain properties, establish a connection between open-loop and closed-loop analysis, and enable the prediction of time-domain performance for reset systems. The accuracy and effectiveness of the proposed methods are successfully validated through simulations and experiments conducted on a reset Proportional-Integral-Derivative (PID) controlled precision motion system.

**Keywords:** Reset control system, Frequency response analysis, Steady state, Closed-loop, Higher-order sinusoidal-input describing functions, Precision motion  
**2000 MSC:** 93C80, 93C10, 70Q05

## 1. Introduction

This paper aims to develop a method for analyzing the frequency response of reset control systems. The development of the reset element starts from the Clegg integrator (CI), introduced in 1958 Clegg (1958). The CI is a linear integrator encapsulating with a reset mechanism, which enables the output of the CI to be reset to zero whenever its input crosses zero. Through the Describing Function (DF) analysis, the CI demonstrates the same gain-frequency characteristics as a linear integrator but exhibits a significant phase lead of 51.9°. This phase-frequency characteristic highlights the ability of the reset element to overcome the Bode gain-phase restriction in linear controllers Chen et al. (2018). Numerous other applications of reset elements showcase their ability to enhance the system performance. These include the First-order Reset Element

(FORE) Krishnan and Horowitz (1974); Horowitz and Rosenbaum (1975), the Second-order Reset Element (SORE) Hazeleger et al. (2016), partial reset techniques Beker et al. (2004), Proportional-Integral (PI) + CI Baños and Vidal (2007), reset control systems with reset bands Baños et al. (2011), Fractional-order Reset Element (FrORE) Saikumar and HosseinNia (2017); Weise et al. (2019, 2020), and Constant in gain Lead in phase (CgLp) Saikumar et al. (2019).

Frequency response analysis is a method used to assess the magnitude and phase properties of a control system by analyzing its steady-state responses to sinusoidal inputs across various frequencies Tian and Gao (2007). Engineers can shape and tune the performance of closed-loop systems based on their open-loop analysis, a technique referred to as loop shaping Van Loon et al. (2017); Ogata (2010). The frequency-domain-based loop shaping approach has proven effective for designing linear control systems, including PID controllers, in industries Saikumar et al. (2019); Deenen et al. (2017); Saikumar et al. (2021). Reset controllers are seamlessly integrated into the classical PID frame-

\*Corresponding author.

Email addresses: X.Zhang-15@tudelft.nl (Xinxin Zhang), MBKaczmarek@tudelft.nl (Marcin B Kaczmarek), S.H.HosseinNiaKani@tudelft.nl (S. Hassan HosseinNia)

work, thus attracting interest for their potential applications across various industries [Beerens et al. \(2021\)](#). However, the lack of effective frequency-domain analysis tools tailored for reset control systems has hindered their widespread adoption in industries.

The frequency response analysis includes both open-loop and closed-loop analysis. For open-loop reset controllers, the DF [Guo et al. \(2009\)](#) was first employed to analyze their frequency response, but it falls short in capturing the complete dynamics of reset control systems as it only analyzes the first harmonic of the outputs. The Higher-Order Sinusoidal Input Describing Function (HOSIDF) [Saikumar et al. \(2021\)](#), which accounts for higher-order harmonics, proves to be an effective method for analyzing open-loop reset control systems. However, in closed-loop reset control systems, the existence of high-order harmonics in the output signals leads to the generation of higher-order sub-harmonics through the feedback loop, presenting challenges for frequency response analysis. Existing tools for analyzing closed-loop reset control systems, such as pseudo-sensitivity functions in [Dastjerdi et al. \(2022\)](#), primarily rely on time-domain approaches and lack a direct connection between open-loop and closed-loop analysis of reset control systems. The current frequency-domain-based analysis method for reset control systems in [Saikumar et al. \(2021\)](#) lacks precision as it overlooks certain higher-order harmonics in the closed-loop outputs.

The lack of precise frequency response analysis methods for closed-loop reset systems and the disconnect between open-loop and closed-loop analysis in reset systems motivates this research. The objective of this research is to develop new frequency response analysis methods for both open-loop and closed-loop reset control systems with sinusoidal inputs. These methods aim to (1) predict the steady-state performance of the closed-loop reset control system by rectifying inaccuracies present in previous methods, and (2) establish a reliable connection between the frequency-domain analysis of the open-loop and closed-loop reset control systems.

The structure of the study is organized as follows. Section 2 provides definitions, discusses existing frequency response analysis methods for reset control systems, and states the research problems. The main contributions are detailed in Section 3 (for the open-loop reset system) and Section 4 (for the closed-loop reset system), including:

1. Theorem 1 presents a new pulse-based approach for analyzing open-loop reset systems. This

method decomposes the steady-state outputs of reset systems into base-linear outputs and pulse-based nonlinear signals. Building on Theorem 1, Theorem 2 proposes an open-loop HOSIDF for the frequency response analysis of reset controllers.

2. Building upon Theorem 2, Theorem 3 introduces an analysis method for a closed-loop Single-Sinusoid-Input Single-Output (SSISO) reset control system featuring two reset instants per steady-state period (referred to as a two-reset system). This model decomposes the system's steady-state output into its base-linear and nonlinear components.
3. Based on Theorem 3, a closed-loop HOSIDF is developed for the frequency response analysis of reset control systems, as detailed in Theorem 4. This analysis connects the open-loop and closed-loop responses of reset control systems, enabling the application of loop-shaping techniques in nonlinear systems for the first time.

Section 5 assesses the accuracy and highlights limitations of the proposed methods on a reset control system within the PID framework, demonstrated through simulations and experiments. In Section 6, we introduce a novel reset control structure aimed at addressing the limitations identified in Section 5. Simulated and experimental results on this new control system validate the effectiveness of the proposed analysis methods. Additionally, this section discusses the applicability of the methods in reset control system design. Finally, the study concludes in Section 7.

## 2. Background and Problem Statement

This section begins by offering background information on reset control systems. It then discusses existing frequency response analysis methods for reset systems, highlighting their limitations. Finally, the research problems are introduced.

### 2.1. The Definition of the Reset Control System

Figure 1 illustrates the block diagram of the Single-Input Single-Output (SISO) reset control system. This system consists of a reset controller  $C$ , a linear controller  $C_a$ , a plant  $\mathcal{P}$ , and a feedback loop. The blue lines depict the resetting mechanism activated by the reset trigger signal (which is  $e(t)$  in this diagram). The signals  $r(t)$ ,  $e(t)$ ,  $v(t)$ ,  $u(t)$ , and  $y(t)$  correspond to the reference input signal, the error signal, the reset output signal, the control input signal, and the output signal,

respectively. Note that in the reset system under a sinusoidal input signal  $r(t) = |R|\sin(\omega t)$  ( $\omega \in \mathbb{R}^+$ ), these signals are functions of both time  $t$  and input frequency  $\omega$ . In the time domain, they are expressed as functions of  $t$  for a specific  $\omega$  for simplicity. Under the condition of the existence of steady states, in the Fourier domain,  $R(\omega)$ ,  $E(\omega)$ ,  $V(\omega)$ ,  $U(\omega)$ , and  $Y(\omega)$  represent their respective Fourier transforms.

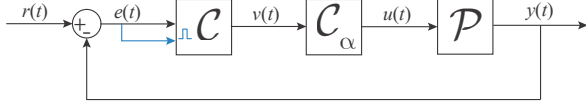


Figure 1: The block diagram of the reset control system, where  $r(t)$ ,  $e(t)$ ,  $v(t)$ ,  $u(t)$ , and  $y(t)$  denote the reference input signal, the error signal, the reset output signal, the control input signal, and the output signal, respectively. The blue lines indicate the reset-triggered actions, with  $e(t)$  serving as the reset-triggered signal in this system.

The state-space equations of the reset controller  $C$  in Fig. 1 are given by:

$$C = \begin{cases} \dot{x}_c(t) = A_R x_c(t) + B_R e(t), & t \notin J, \\ x_c(t^+) = A_\rho x_c(t), & t \in J, \\ v(t) = C_R x_c(t) + D_R e(t). \end{cases} \quad (1)$$

In (1),  $x_c(t) \in \mathbb{R}^{n_c \times 1}$  represents the state of the reset controller  $C$ , where  $n_c$  denotes the number of states. The matrices  $A_R \in \mathbb{R}^{n_c \times n_c}$ ,  $B_R \in \mathbb{R}^{n_c \times 1}$ ,  $C_R \in \mathbb{R}^{1 \times n_c}$ , and  $D_R \in \mathbb{R}^{1 \times 1}$  describe the continuous dynamics of the base-linear controller (BLC), denoted as  $C_{bl}(\omega)$ , given by

$$C_{bl}(\omega) = C_R(j\omega I - A_R)^{-1} B_R + D_R, \quad (j = \sqrt{-1}). \quad (2)$$

The base-linear system (BLS) of the reset control system in Fig. 1 is the system characterized by substituting the reset controller  $C$  with its base-linear counterpart  $C_{bl}$ .

The reset controller employs the ‘‘zero-crossing law’’ as the reset mechanism, which enables the state  $x_c(t)$  of  $C$  resets to a predetermined value whenever the reset-triggered signal crosses zero [Banos and Barreiro \(2012\)](#); [Guo and Chen \(2019\)](#). In Fig. 1, the reset triggered signal is  $e(t)$ . The second equation in (1) describes the reset action, which is an instantaneous or impulsive change of the state ( $x_c(t) \rightarrow x_c(t^+)$ ) applied whenever  $e(t_i) = 0$  [Barreiro et al. \(2014\)](#). The reset instant, denoted as  $t_i$ , is defined as the time at which the reset condition is satisfied, i.e.,  $e(t_i) = 0$ . The set of reset instants for  $C$  is defined as  $J := \{t_i | e(t_i) = 0, i \in \mathbb{Z}^+\}$ . The symbol  $A_\rho$  represents the reset matrix, given by

$$A_\rho = \begin{bmatrix} \gamma & \\ & I_{n_i} \end{bmatrix} \in \mathbb{R}^{n_c \times n_c}, \quad (3)$$

where  $\gamma = \text{diag}(\gamma_1, \gamma_2, \dots, \gamma_o, \dots, \gamma_{n_r})$ ,  $o \in \mathbb{Z}^+$ .  $\gamma_o \in (-1, 1)$  denotes the ratio of the after-reset state value (at  $t_i^+$ ) to the before-reset state value (at  $t_i$ ). The subscripts  $n_r$  and  $n_l$  denote the numbers of reset states and non-reset (linear) states, respectively, where  $n_c = n_r + n_l$ . When  $\gamma = I_{n_r}$ , the reset controller  $C$  is referred to as its BLC  $C_{bl}$ . In this study, we specifically focus on the reset controller  $C$  that employs the ‘‘Zero-crossing Law’’ and involves a single reset state, where  $n_r = 1$  in (3). The reset controllers with  $n_r = 1$  encompass common elements such as the CI, the FORE, and the higher-order reset elements like the ‘‘Second-Order Single State Reset Element (SOSRE)’’ [Karbasizadeh et al. \(2021\)](#).

In Fig. 1, the linear controller  $C_\alpha$  combined with the plant  $\mathcal{P}$  is defined as  $\mathcal{P}_\alpha = C_\alpha \mathcal{P}$ . The state-space representation of  $\mathcal{P}_\alpha$  is defined as:

$$\mathcal{P}_\alpha = \begin{cases} \dot{x}_\alpha(t) = A_\alpha x_\alpha(t) + B_\alpha v(t), \\ y_\alpha(t) = C_\alpha x_\alpha(t), \end{cases} \quad (4)$$

where  $A_\alpha \in \mathbb{R}^{n_\alpha \times n_\alpha}$ ,  $B_\alpha \in \mathbb{R}^{n_\alpha \times 1}$ , and  $C_\alpha \in \mathbb{R}^{1 \times n_\alpha}$  are the state-space matrices for  $\mathcal{P}_\alpha$ .  $x_\alpha \in \mathbb{R}^{n_\alpha \times 1}$  represents the state of  $\mathcal{P}_\alpha$  and  $n_\alpha \in \mathbb{N}$  is the number of the state.

Combining (1) and (4), the state-space representative of the reset control system without inputs is given by

$$\mathcal{H} = \begin{cases} \dot{x}(t) = A_{cl} x(t), & x \notin J_H, \\ x(t^+) = A_{\rho cl} x(t), & x \in J_H, \\ y(t) = C_{cl} x(t), \end{cases} \quad (5)$$

where  $x^T = [x_c^T \ x_\alpha^T] \in \mathbb{R}^{n_s \times 1}$  is the state of the reset control system  $\mathcal{H}$ , with the number of  $n_s = n_c + n_\alpha$ .  $J_H := \{x \in \mathbb{R}^{n_s \times 1} | C_{cl} x = 0\}$  is defined to be the set of reset instants satisfying  $e(t) = 0$ . The matrices in (5) are given by

$$\begin{aligned} A_{cl} &= \begin{bmatrix} A_R & -B_R C_\alpha \\ B_\alpha C_R & A_\alpha \end{bmatrix} \in \mathbb{R}^{n_s \times n_s}, \\ C_{cl} &= \begin{bmatrix} 0^{1 \times n_c} & C_\alpha \end{bmatrix} \in \mathbb{R}^{1 \times n_s}, \\ A_{\rho cl} &= \begin{bmatrix} A_\rho & 0 \\ 0 & I_{n_\alpha} \end{bmatrix} \in \mathbb{R}^{n_s \times n_s}. \end{aligned} \quad (6)$$

## 2.2. Current Frequency Response Analysis of the Open-loop Reset System

The stability and convergence of systems are crucial for achieving a steady-state solution and enabling frequency response to sinusoidal inputs [Pavlov et al. \(2006, 2007\)](#). An open-loop reset system (1) with input signal of  $e(t) = |E|\sin(\omega t + \angle E)$  has a globally asymptotically stable  $2\pi/\omega$ -periodic solution if and only if [Guo et al. \(2009\)](#))

$$|\lambda(D_R e^{A_R \delta})| < 1, \quad \forall \delta \in \mathbb{R}^+. \quad (7)$$

Thus, we have the following assumption:

**Assumption 1.** The reset system (1) with input  $e(t) = |E|\sin(\omega t + \angle E)$  is assumed to meet the condition in (7).

Regarding the Zeno-ness problem in the hybrid system, the outputs for the reset system are Zeno-free if the reset time interval  $\sigma_i = t_{i+1} - t_i$ ,  $i \in \mathbb{Z}^+$ , between any two consecutive reset instants  $(t_i, t_{i+1})$ , is lower bounded.

$$\sigma_i > \sigma_{\min}, \quad (8)$$

at least in some working domain  $\Omega$  Barreiro et al. (2014).

For an open-loop reset controller  $C$  (1), with the input signal and the reset triggered signal of  $e(t) = |E|\sin(\omega t)$  and satisfying Assumption 1, there exist  $n \in \mathbb{N}$  harmonics in the reset output signal  $v(t)$ . Utilizing the ‘‘Virtual Harmonic Generator’’ Heinen (2018), the input signal  $e(t)$  generates  $n$  harmonics  $e_{1n}(t) = |E|\sin(n\omega t)$ . The function  $H_n(\omega)$ , where  $n$  denotes the number of harmonics involved, is defined to represent the transfer function from  $e_{1n}(t)$  to the  $n$ -th harmonic in  $v(t)$  at steady states. The expression for  $H_n(\omega)$  is provided by Heinen (2018); Saikumar et al. (2021):

$$H_n(\omega) = \begin{cases} C_R(j\omega I - A_R)^{-1}(I + j\Theta_D(\omega))B_R + D_R, & \text{for } n = 1, \\ C_R(jn\omega I - A_R)^{-1}j\Theta_D(\omega)B_R, & \text{for odd } n > 1, \\ 0, & \text{for even } n \geq 2, \end{cases} \quad (9)$$

with

$$\begin{aligned} \Lambda(\omega) &= \omega^2 I + A_R^2, \\ \Delta(\omega) &= I + e^{(\frac{\pi}{\omega} A_R)}, \\ \Delta_r(\omega) &= I + A_\rho e^{(\frac{\pi}{\omega} A_R)}, \\ \Gamma_r(\omega) &= \Delta_r^{-1}(\omega) A_\rho \Delta(\omega) \Lambda^{-1}(\omega), \\ \Theta_D(\omega) &= \frac{-2\omega^2}{\pi} \Delta(\omega) [\Gamma_r(\omega) - \Lambda^{-1}(\omega)]. \end{aligned} \quad (10)$$

Note that the expression for the first-order harmonic  $H_1(\omega)$  aligns with the classical DF representation for the reset controller in Guo et al. (2009).

### 2.3. The Stability and Convergence Conditions of the Closed-loop Reset System

For the frequency response analysis of closed-loop reset control systems, stability and convergence conditions are also necessary. The closed-loop reset control system (5) is quadratically stable if and only if it satisfies the well-known  $H_\beta$  condition Beker et al. (2004); Carrasco et al. (2008), i.e., there exists a  $\beta \in \mathbb{R}^{n_r \times 1}$  and a

positive definite matrix  $P_{n_r} \in \mathbb{R}^{n_r \times n_r}$  such that the transfer function

$$H_\beta(s) \triangleq \begin{bmatrix} P_{n_r} & 0_{n_r \times n_l} & \beta C_\alpha \end{bmatrix} (sI - A_{cl})^{-1} \begin{bmatrix} I_{n_r} \\ 0_{n_l \times n_r} \\ 0_{n_a \times n_r} \end{bmatrix} \quad (11)$$

is strictly positive real and additionally a non-zero reset matrix  $A_{\rho r}$  satisfies the condition

$$A_{\rho r}^T P_{n_r} A_{\rho r} - P_{n_r} \leq 0, \quad (12)$$

where  $I_{n_r}$  is an identity matrix of size  $n_r \times n_r$ .

Literature Dastjerdi et al. (2022) proposed that the closed-loop reset control system (5) is uniformly exponentially convergent if the initial condition of the reset controller is zero, there are infinitely many reset instants  $t_i$  with  $\lim_{t_i \rightarrow \infty} t_i = \infty$ , the input signal  $r(t)$  is a Bohl function Barabanov and Konyukh (2001), and the  $H_\beta$  condition is satisfied Dastjerdi et al. (2022); Hollot et al. (2001). Additionally, when these convergent conditions are met, the closed-loop reset control system (5) under sinusoidal input signal  $r(t) = |R|\sin(\omega t)$  exhibits a periodic steady-state solution. This solution can be represented as  $x(t) = \mathcal{S}(\sin(\omega t), \cos(\omega t), \omega)$  for some function  $\mathcal{S} : \mathbb{R}^3 \rightarrow \mathbb{R}^{n_c + n_a}$  Dastjerdi et al. (2022).

Considering the stability, convergence, and the existence of steady-state is needed for the frequency response analysis for the closed-loop system, we have the following Assumption 2.

**Assumption 2.** The closed-loop reset control system (5) is assumed to satisfy the following conditions: the initial condition of the reset controller  $C$  is zero, there are infinitely many reset instants  $t_i$  with  $\lim_{t_i \rightarrow \infty} t_i = \infty$ , the input signal is a Bohl function, Barabanov and Konyukh (2001), there is no Zenoness behaviour, and the  $H_\beta$  condition (in (11) and (12)) is satisfied.

Note that Assumption 2 can be met through appropriate design considerations, see Saikumar et al. (2021); Banos and Barreiro (2012); Samad et al. (2019).

### 2.4. Problem Statement

Under Assumption 2, in a SISO closed-loop reset control system with a sinusoidal reference input signal  $r(t) = |R|\sin(\omega t)$  (in Fig. 1), the steady-state signals  $e(t)$ ,  $v(t)$ ,  $u(t)$ , and  $y(t)$  are periodic and nonlinear. The Fourier transformations of these signals are define as  $E(\omega)$ ,  $V(\omega)$ ,  $U(\omega)$ , and  $Y(\omega)$ , respectively. These signals encompass infinite harmonics and share the fundamental frequency of  $r(t)$  Pavlov et al. (2006). They can

be expressed as follows:

$$\begin{aligned}
e(t) &= \sum_{n=1}^{\infty} e_n(t) = \sum_{n=1}^{\infty} |E_n| \sin(n\omega t + \angle E_n), \\
v(t) &= \sum_{n=1}^{\infty} v_n(t) = \sum_{n=1}^{\infty} |V_n| \sin(n\omega t + \angle V_n), \\
u(t) &= \sum_{n=1}^{\infty} u_n(t) = \sum_{n=1}^{\infty} |U_n| \sin(n\omega t + \angle U_n), \\
y(t) &= \sum_{n=1}^{\infty} y_n(t) = \sum_{n=1}^{\infty} |Y_n| \sin(n\omega t + \angle Y_n),
\end{aligned} \tag{13}$$

where  $\angle E_n, \angle V_n, \angle U_n, \angle Y_n \in (-\pi, \pi]$ . The signals  $e_n(t)$ ,  $v_n(t)$ ,  $u_n(t)$  and  $y_n(t)$  are the  $n^{\text{th}}$  harmonics of  $e(t)$ ,  $v(t)$ ,  $u(t)$  and  $y(t)$ , respectively. The Fourier transformations of these signals are define as  $E_n(\omega)$ ,  $V_n(\omega)$ ,  $U_n(\omega)$ , and  $Y_n(\omega)$ , respectively.

Conducting a frequency response analysis serves as an effective tool not only for understanding the frequency-domain dynamics of the system [Saikumar et al. \(2021\)](#), but also for predicting the performance of the closed-loop reset control system. For instance, the steady-state error  $e(t)$  in (13) serves as an important metric in assessing the tracking precision of the system. Currently, two frequency response analysis methods for closed-loop reset control systems are available, denoted as Method A and Method B.

Method A ([Guo et al. \(2009\)](#)): For a SISO reset system with a reference input signal  $r(t) = |R| \sin(\omega t)$  under Assumption 2, as shown in Fig. 1, the sensitivity function  $\mathcal{S}_{DF}(\omega)$ , complementary sensitivity function  $\mathcal{T}_{DF}(\omega)$ , and control sensitivity function  $\mathcal{CS}_{DF}(\omega)$  based on the steady-state DF analysis are defined as

$$\begin{aligned}
\mathcal{S}_{DF}(\omega) &= \frac{E(\omega)}{R(\omega)} = \frac{1}{1 + H_1(\omega)C_\alpha(\omega)\mathcal{P}(\omega)}, \\
\mathcal{T}_{DF}(\omega) &= \frac{Y(\omega)}{R(\omega)} = \frac{H_1(\omega)\mathcal{P}(\omega)}{1 + H_1(\omega)C_\alpha(\omega)\mathcal{P}(\omega)}, \\
\mathcal{CS}_{DF}(\omega) &= \frac{U(\omega)}{R(\omega)} = \frac{H_1(\omega)C_\alpha(\omega)}{1 + H_1(\omega)C_\alpha(\omega)\mathcal{P}(\omega)},
\end{aligned} \tag{14}$$

where  $H_1(\omega)$  represents the first-order harmonic transfer function of  $C$ , as defined in (9). However, Method A is inaccurate for predicting the performance of closed-loop reset control systems since it only considers the first-order harmonic of the reset control system, thus being valid only when  $e_n(t) = 0$  for  $n > 1$  in (13). In contrast, the following Method B incorporates the higher-order harmonics, which is more accurate.

Method B ([Saikumar et al. \(2021\)](#)): For a SISO reset control system in Fig. 1 with a reference input signal  $r(t) = |R| \sin(\omega t)$ , under three assumptions: 1) Assumption 2, 2) the reset triggered signal is  $e_1(t)$  which results in two reset instants occurring  $\pi/\omega$  apart per cycle, and 3) the error  $e_n(t)$  for  $n > 1$  does not undergo reset actions, the  $n^{\text{th}}$  ( $n \in \mathbb{N}$ ) steady-state sensitivity function,

complementary sensitivity function, and control sensitivity function denoted as  $\mathcal{S}_n(\omega)$ ,  $\mathcal{T}_n(\omega)$ , and  $\mathcal{CS}_n(\omega)$  are given by

$$\begin{aligned}
\mathcal{S}_n(\omega) &= \frac{E_n(n\omega)}{R_n(\omega)} \\
&= \begin{cases} \mathcal{S}_{11}(\omega), & \text{for } n = 1, \\ -\mathcal{L}_n(\omega)\mathcal{S}_{bl}(n\omega)(|\mathcal{S}_{11}(\omega)| \angle(n\angle\mathcal{S}_{11}(\omega))), & \text{for odd } n > 2, \\ 0, & \text{for even } n \geq 2, \end{cases} \\
\mathcal{T}_n(\omega) &= \frac{Y_n(n\omega)}{R_n(\omega)} \\
&= \begin{cases} 1 - \mathcal{S}_{11}(\omega), & \text{for } n = 1, \\ \mathcal{L}_n(\omega)\mathcal{S}_{bl}(n\omega)(|\mathcal{S}_{11}(\omega)| \angle(n\angle\mathcal{S}_{11}(\omega))), & \text{for odd } n > 2, \\ 0, & \text{for even } n \geq 2, \end{cases} \\
\mathcal{CS}_n(\omega) &= \frac{U_n(n\omega)}{R_n(\omega)} = \mathcal{T}_n(\omega)/\mathcal{P}(n\omega),
\end{aligned} \tag{15}$$

where

$$\begin{aligned}
\mathcal{S}_{11}(\omega) &= 1/(1 + \mathcal{L}_n(\omega)), \\
R_n(\omega) &= |R| \mathcal{F}[\sin(n\omega t)], \\
\mathcal{S}_{bl}(n\omega) &= 1/(1 + \mathcal{L}_{bl}(n\omega)), \\
\mathcal{L}_n(\omega) &= H_n(\omega)C_\alpha(n\omega)\mathcal{P}(n\omega), \\
\mathcal{L}_{bl}(n\omega) &= C_{bl}(n\omega)C_\alpha(n\omega)\mathcal{P}(n\omega).
\end{aligned} \tag{16}$$

Note that the first-order harmonic in Method B is identical to Method A. Although Method B takes the higher-order harmonics (for  $n > 1$ ) into consideration, the Assumption 3) overlooks the higher-order harmonics generated by  $e_n(t)$  ( $n > 1$ ) in (13). This oversight will result in analysis inaccuracies, motivating the contributions made in this paper.

The main idea of this paper is to introduce a new method for analyzing the frequency response of closed-loop SISO reset control systems. It begins with open-loop analysis of reset controllers. The open-loop analysis decomposes the steady-state outputs of reset controllers into base-linear and pulse-based nonlinear elements. This decomposition approach facilitates the development of frequency responses for closed-loop reset control systems, correcting inaccurate assumptions Assumption 3) in Method B [Saikumar et al. \(2021\)](#). The proposed methods serve as tools for conducting frequency-domain analysis and predicting time-domain performance for reset systems.

### 3. The Frequency Response Analysis for the Open-loop Reset System

This section introduces a pulse-based analysis model for the open-loop reset controller at syeady states. The model separates the output of a SSISO reset controller into its base-linear sinusoidal output and a filtered pulse

signal. The term ‘‘filtered pulse signal’’ refers to a signal obtained by filtering a normalized pulse signal through a finite-dimensional transfer function.

The reset controller  $C$  (1) is built on the primitive CI [Banos and Barreiro \(2012\)](#). To establish the analysis model for the general reset controller, we begin with analyzing the CI. The Generalized CI (GCI) is defined as the reset controller  $C$  (1) with  $A_R = 0$ ,  $B_R = 1$ ,  $C_R = 1$ ,  $D_R = 0$ , and  $A_p = \gamma \in (-1, 1)$ , under Assumption 1 and the Zeno-free condition in (8). Lemma 1 illustrates that the GCI’s output comprises the summation of its base-linear output and a square wave component.

**Lemma 1.** (The pulse-based model for the open-loop GCI) For a GCI subjected to a sinusoidal input signal  $e(t) = |E_1|\sin(\omega t)$ , its steady-state output signal denoted by  $u_{ci}(t)$  consists of two components: one is its base-linear output  $u_i(t)$  and another is a square wave represented as  $q_i(t)$ , expressed by:

$$u_{ci}(t) = u_i(t) + q_i(t), \quad (17)$$

where  $u_i(t) = -|E_1|/\omega[\cos(\omega t) - 1]$ , and  $q_i(t)$  is a  $2\pi/\omega$ -periodical square wave given by

$$q_i(t) = \begin{cases} -2|E_1|\gamma(\gamma + 1)^{-1}/\omega, & \text{for } t \in [2k, 2k + 1) \cdot \pi/\omega, \\ -2|E_1|(\gamma + 1)^{-1}/\omega, & \text{for } t \in [2k + 1, 2k + 2) \cdot \pi/\omega, \end{cases} \quad (18)$$

where  $k \in \mathbb{N}$ .

*Proof.* The proof can be found in [Appendix A](#).  $\square$

Figure 2 displays the simulation results of an open-loop CI with the input signal  $e(t) = \sin(\omega t)$  ( $\omega = \pi$  rad/s and  $\gamma = 0$ ). In this case,  $q_i(t)$  is a square wave with a period of 2 s and amplitudes of 0 and 0.64, as calculated by (18).

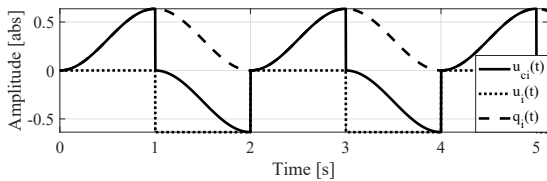


Figure 2:  $u_{ci}(t)$  (solid line),  $u_i(t)$  (dotted line), and  $q_i(t)$  (dashed line) of open-loop CI.

Theorem 1 extends the pulse-based analysis model from the GCI to a open-loop reset controller  $C$  (1) under different input and reset-triggered signals.

**Theorem 1.** (The pulse-based analysis model for the open-loop reset controller) Consider a reset controller  $C$  described by (1), where  $n_r = 1$ , subject to a sinusoidal

input signal  $e(t) = |E_n|\sin(\omega t + \angle E_n)$  with  $\angle E_n \in (-\pi, \pi]$  and  $n = 2k + 1$  for  $k \in \mathbb{N}$ , along with a  $2\pi/\omega$ -periodic reset triggered signal denoted by  $e_s(t) = |E_s|\sin(\omega t + \angle E_s)$ , where  $\angle E_s \in (-\pi, \pi]$ , under Assumption 1 and adhere to the Zeno-free condition outlined in (8). The input signal  $e(t) = |E_n|\sin(\omega t + \angle E_n)$  varies as a function of time  $t$ , while the parameters  $\omega$  and  $n$  remain constant. The steady-state reset output  $v(t)$  is expressed as:

$$v(t) = v_{bl}(t) + v_{nl}(t), \quad (19)$$

where  $v_{bl}(t)$  is the steady-state base-linear output given by

$$v_{bl}(t) = |E_n C_{bl}(n\omega)|\sin(n\omega t + \angle E_n + \angle C_{bl}(n\omega)). \quad (20)$$

The nonlinear signal  $v_{nl}(t)$  shares the same phase and period as the reset-triggered signal  $e_s(t)$ , as obtained by

$$v_{nl}(t) = \sum_{\mu=1}^{\infty} \mathcal{F}^{-1}[\Delta_x(\mu\omega)Q^\mu(\omega)], \quad \mu = 2k + 1, \quad k \in \mathbb{N}, \quad (21)$$

where

$$\begin{aligned} \Delta_l(n\omega) &= (jn\omega I - A_R)^{-1} B_R, \\ \Delta_x(\mu\omega) &= C_R(j\mu\omega I - A_R)^{-1} j\mu\omega I, \\ \Delta_c^n(\omega) &= |\Delta_l(n\omega)|\sin(\angle \Delta_l(n\omega) + \angle E_n - n\angle E_s), \\ Q^\mu(\omega) &= 2|E_n|\Delta_q^n(\omega)\mathcal{F}[\sin(\mu\omega t + \mu\angle E_s)]/(\mu\pi), \\ \Delta_q^n(\omega) &= (I + e^{A_R\pi/\omega})(A_p e^{A_R\pi/\omega} - I)^{-1}(I - A_p)\Delta_c^n(\omega). \end{aligned} \quad (22)$$

*Proof.* The proof is provided in [Appendix B](#).  $\square$

The reset controller  $C$  in Fig. 1 with the same input signal and reset-triggered signal  $e(t) = |E_1|\sin(\omega t + \angle E_1)$ , corresponds to the reset controller discussed in Theorem 1 when  $e_s(t) = e(t)$ . Based on Theorem 1, Theorem 2 presents the Higher-order Sinusoidal Input Describing Function (HOSIDF) for the open-loop reset controller  $C$  in Fig. 1. The block diagram for  $C$  based on the HOSIDF analysis is depicted in Fig. 3.

**Theorem 2.** (The HOSIDF for the open-loop reset controller) Consider a reset controller  $C$  (1) with one reset state where  $n_r = 1$  in response to the input signal and reset-triggered signal  $e(t) = |E_1|\sin(\omega t + \angle E_1)$ , ( $\angle E_1 \in (-\pi, \pi]$ ), operating under Assumption 1 and satisfying the Zeno-free condition in (8). The steady-state output signal  $v(t)$  comprises  $n \in \mathbb{N}$  harmonics, expressed as  $v(t) = \sum_{n=1}^{\infty} v_n(t)$ , with the Fourier transform defined as  $V(\omega) = \sum_{n=1}^{\infty} V_n(\omega)$ . In Fig. 3, the application of the ‘‘Virtual Harmonic Generator’’ [Saikumar et al. \(2021\)](#); [Nuij et al. \(2006\)](#) introduces  $e_{1n}(t) = |E_1|\sin(n\omega t + n\angle E_1)$ , with Fourier transform denoted as

$E_{1n}(\omega)$ . The  $n$ -th steady-state transfer function of  $C$ , denoted as  $C_n(\omega)$ , represents the ratio of  $V_n(\omega)$  to  $E_{1n}(\omega)$  and is given by:

$$C_n(\omega) = \frac{V_n(\omega)}{E_{1n}(\omega)} = \begin{cases} C_{bl}(\omega) + C_{nl}(\omega), & \text{for } n = 1, \\ C_{nl}(n\omega), & \text{for odd } n > 1, \\ 0, & \text{for even } n \geq 2. \end{cases} \quad (23)$$

where  $C_{bl}(\omega)$  is the base-linear transfer function given in (2) and  $C_{nl}(n\omega)$  is derived by

$$\begin{aligned} \Delta_l(\omega) &= (j\omega I - A_R)^{-1} B_R, \\ \Delta_q(\omega) &= (I + e^{A_R \pi/\omega}) \Delta_v(\omega), \\ \Delta_c(\omega) &= |\Delta_l(\omega)| \sin(\angle \Delta_l(\omega)), \\ C_{nl}(n\omega) &= 2\Delta_x(n\omega) \Delta_q(\omega) / (n\pi), \\ \Delta_x(n\omega) &= C_R(jn\omega I - A_R)^{-1} jn\omega I, \\ \Delta_v(\omega) &= (A_\rho e^{A_R \pi/\omega} - I)^{-1} (I - A_\rho) \Delta_c(\omega). \end{aligned} \quad (24)$$

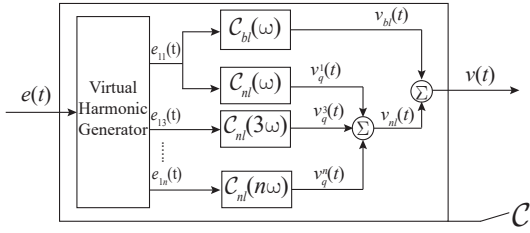


Figure 3: The new block diagram of an open-loop reset controller  $C$ .

*Proof.* The proof can be found in Appendix C.  $\square$

**Corollary 1.** Consider a reset controller  $C$  (1) with one reset state where  $n_r = 1$  in response to the input signal and reset-triggered signal  $e(t) = |E_1| \sin(\omega t + \angle E_1)$ , ( $\angle E_1 \in (-\pi, \pi)$ ). The reset controller  $C$  (1) operates under Assumption 1 and satisfies the Zeno-free condition in (8). The steady-state reset output signal  $v(t)$  is expressed as:

$$v(t) = v_{bl}(t) + v_{nl}(t), \quad (25)$$

where  $v_{bl}(t)$  is the steady-state base-linear output given by

$$v_{bl}(t) = |E_1 C_{bl}(\omega)| \sin(\omega t + \angle C_{bl}(\omega)). \quad (26)$$

The nonlinear signal  $v_{nl}(t)$  is given by

$$v_{nl}(t) = \sum_{n=1}^{\infty} \mathcal{F}^{-1}[E_{1n}(\omega) C_{nl}(n\omega)]. \quad (27)$$

*Proof.* The proof is provided in Appendix D.  $\square$

Note that our earlier work Kaczmarek et al. (2022) conceptualized the pulse-based model for the open-loop reset controller but did not conclude with a frequency-domain analysis for this controller. Theorem 2 completes this research and presents a new HOSIDF for analyzing the open-loop reset controller.

Applying Theorem 2, Remark 1 provides the analysis for the open-loop reset control system in Fig. 1.

**Remark 1.** For an open-loop reset control system in Fig. 1 with the sinusoidal input signal  $e(t) = |E_1| \sin(\omega t + \angle E_1)$  and under Assumption 1, the transfer function  $\mathcal{L}_n(\omega)$ ,  $n \in \mathbb{N}$  from the input  $e(t)$  to the steady-state output  $y(t)$  is composed of a linear transfer function  $\mathcal{L}_{bl}(\omega)$  and nonlinear transfer functions  $\mathcal{L}_{nl}(n\omega)$ , given by

$$\mathcal{L}_n(\omega) = \begin{cases} \mathcal{L}_{bl}(\omega) + \mathcal{L}_{nl}(\omega), & \text{for } n = 1 \\ \mathcal{L}_{nl}(n\omega), & \text{for odd } n > 1 \\ 0, & \text{for even } n \geq 2 \end{cases} \quad (28)$$

with

$$\begin{aligned} \mathcal{L}_{bl}(n\omega) &= C_{bl}(n\omega) C_\alpha(n\omega) \mathcal{P}(n\omega), \\ \mathcal{L}_{nl}(n\omega) &= C_{nl}(n\omega) C_\alpha(n\omega) \mathcal{P}(n\omega), \end{aligned} \quad (29)$$

where  $C_{bl}(n\omega)$  and  $C_{nl}(n\omega)$  are given in (2) and (24), respectively.

The steady-state output signal  $y(t)$  of the open-loop reset system is given by

$$\begin{aligned} y(t) &= \mathcal{F}^{-1}[E_{1n}(\omega) \mathcal{L}_n(\omega)], \\ E_{1n}(\omega) &= |E_1| \sin(n\omega t + n\angle E_1). \end{aligned} \quad (30)$$

To validate the accuracy of Theorem 2 and Remark 1, Fig. 4 compares the simulated and equation (30)-predicted output signals  $y(t)$  in a reset control system with input signal of  $e(t) = \sin(400\pi t)$ . The parameters of the system are given as:  $C_{bl}(s) = 1/(s/(300\pi) + 1)$ ,  $C_\alpha(s) = (s/(75\pi) + 1)/(s/(1200\pi) + 1)$ ,  $\mathcal{P}(s) = 1$ , and  $\gamma = 0$ .

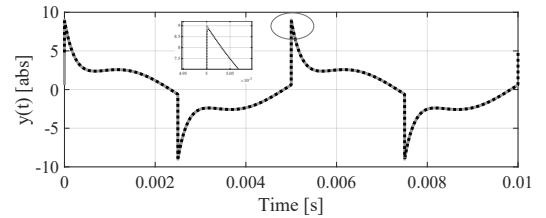


Figure 4: The comparison between the simulated and the Theorem 2-predicted output signals in a reset control system.

The results demonstrate the accuracy of Theorem 2 and Remark 1. Note that that in the zoom-in plot, the slight discrepancy at the signal edges between the two

plots arises from the consideration of 5000 harmonics during the calculation process, whereas the actual output comprises an infinite number of harmonics. The choice of the number of harmonics considered in the calculation allows readers to balance computation time and prediction precision.

The newly introduced HOSIDF  $C_n(\omega)$  (23) is mathematically equivalent to the function  $H_n(\omega)$  (9) when the input signal and reset-triggered signal for the reset controller are the same, denoted as  $e(t) = |E_1|\sin(\omega t + \angle E_1)$ . However, the new HOSIDF offers several new insights: (1) It facilitates the separation of the output  $v(t)$  of the reset controller into linear  $v_{bl}(t)$  (26) and nonlinear  $v_{nl}(t)$  (27) components. Specifically,  $v_{bl}(t)$  is derived from the base-linear transfer function  $C_{bl}(\omega)$  (2), while  $v_{nl}(t)$  is obtained from  $C_{nl}(n\omega)$  (24). (2) The nonlinear signal  $v_{nl}(t)$  is a filtered pulse signal that shares the same phase and period as the reset-triggered signal  $e_s(t)$ . (3) The magnitude of the signal  $v_{nl}(t)$  is determined by  $C_{nl}(n\omega)$ . These insights enable the connection between open-loop analysis and closed-loop frequency analysis, as discussed in Section 4.

#### 4. The Frequency Response Analysis for the Closed-loop Reset System

Based on the open-loop analysis in Theorem 2, this section develops the closed-loop frequency response analysis for the reset control depicted in Fig. 1.

In a closed-loop reset control system under a sinusoidal input signal  $r(t) = |R|\sin(\omega t)$  at steady states, a “two-reset system” is defined as a reset system having two reset instants per steady-state cycle, while a “multiple-reset system” involves more than two reset instants per steady-state cycle. In the two-reset system, the dominated component of the error signal  $e(t)$  is the first-order harmonic  $e_1(t)$  in (13). Multiple-reset actions, such as those implemented in the PI+CI control system, introduce excessive higher-order harmonics compared to two-reset actions Baños and Vidal (2007). This issue can be mitigated through careful design considerations Saikumar et al. (2019); Karbasizadeh et al. (2020). Conditions for achieving periodic output in a multiple-reset system, where the interval between successive resets is not constant, are discussed in Beker (2001). Classical DF also assumes the  $e_1(t)$  results in reset actions. Moreover, based on the authors’ best knowledge, most practical reset control systems in the literature are designed to take advantage of two-reset systems Banos and Barreiro (2012). Given these insights, it is essential to explore frequency-domain analysis methods

tailored to two-reset systems. Hence, we introduce the following assumption.

**Assumption 3.** There are two reset instants in a SISO closed-loop reset control system with a sinusoidal reference input signal  $r(t) = |R|\sin(\omega t)$  at steady states, where the reset-triggered signal is  $e_1(t)$ .

Note that achieving Assumption 3 is feasible through practical reset control design. For instance, the CgLp reset element introduced in Saikumar et al. (2019) enables the realization of wide-band two-reset systems. The analysis of multiple-reset systems extends beyond the current scope and will be the focus of our future research.

Under Assumptions 2 and 3, the reset actions in the closed-loop SISO reset control system occur when  $e_1(t) = |E_1|\sin(\omega t + \angle E_1) = 0$ , where  $\angle E_1 \in (-\pi, \pi]$ . The set of reset instants for this closed-loop reset system is denoted as  $J_m := \{t_m = (m\pi - \angle E_1)/\omega | m \in \mathbb{Z}^+\}$ . Since the reset interval  $\sigma_m = t_{m+1} - t_m = \pi/\omega > \delta_{\min}$  Barreiro et al. (2014), the trajectories for the reset system are Zeno-free.

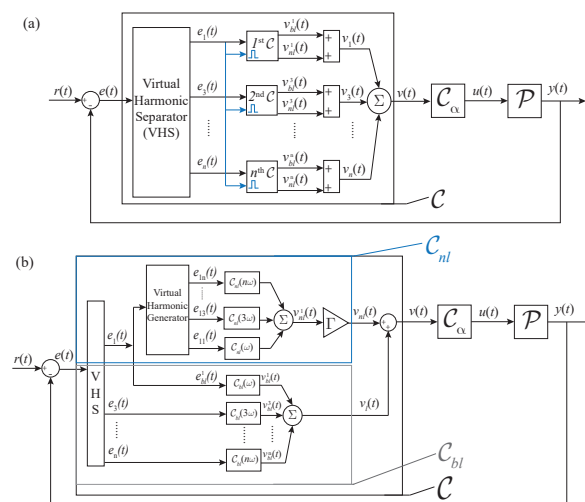


Figure 5: Block diagrams for the closed-loop RCS, wherein (a) the resetting actions are indicated by the blue lines. In (b), the reset controller is decomposed into two components: the linear part  $C_{bl}$  within the grey box and the nonlinear part  $C_{nl}$  contained within the blue box.

Figure 5(a) constructs the first block diagram for the closed-loop reset control system under Assumptions 2 and 3. In this block diagram, first, utilizing the “Virtual Harmonic Separator” Nuij et al. (2006), the error signal  $e(t)$  is decomposed into its harmonics,  $e_n(t)$ , as defined in (13). Next, each  $e_n(t)$  is filtered by the reset controller  $C$ , resulting in a response denoted as  $v_n(t)$ . By summing up  $v_n(t)$ , the reset output signal  $v(t)$  is obtained. In this



context, we refer to  $C$  with the input signal  $e_n(t)$  as the  $n$ -th reset controller. Theorem 1 illustrates that the steady-state output of a reset controller  $C$  under a sinusoidal input signal is composed of base-linear  $v_{bl}(t)$  and non-linear  $v_{nl}(t)$  components. Let  $v_{bl}^n(t)$  and  $v_{nl}^n(t)$  represent the steady-state base-linear and nonlinear output signals for the  $n$ -th  $C$ . Then, the steady-state reset output signal  $v(t)$  in the closed-loop reset system is given by:

$$\begin{aligned} v(t) &= \sum_{n=1}^{\infty} v_n(t), \\ v_n(t) &= v_{bl}^n(t) + v_{nl}^n(t). \end{aligned} \quad (31)$$

From (31), by defining

$$\begin{aligned} v_l(t) &= \sum_{n=1}^{\infty} v_{bl}^n(t), \\ v_{nl}(t) &= \sum_{n=1}^{\infty} v_{nl}^n(t), \end{aligned} \quad (32)$$

$v(t)$  can be written as

$$v(t) = v_l(t) + v_{nl}(t). \quad (33)$$

In the Fourier domain, equation (31) is expressed as

$$\begin{aligned} V(\omega) &= \sum_{n=1}^{\infty} V_n(\omega), \\ V_n(\omega) &= V_{bl}^n(\omega) + V_{nl}^n(\omega). \end{aligned} \quad (34)$$

Derived from (20),  $V_{bl}^n(\omega)$  is given by

$$V_{bl}^n(\omega) = E_n(\omega)C_{bl}(n\omega). \quad (35)$$

Based on the block diagram for the closed-loop reset system shown in Fig. 5(a), Theorem 3 concludes the development of the pulse-based model for the closed-loop reset control system, visually represented in Fig. 5(b).

**Theorem 3.** (The pulse-based analysis model for the closed-loop reset system) In a closed-loop reset control system (with reset controller  $C$  (1) where  $n_r = 1$ ), as depicted in Fig. 1 with a sinusoidal reference input signal  $r(t) = |R|\sin(\omega t)$  and under Assumptions 2 and 3, the steady-state reset output signal  $v(t)$  is expressed as:

$$\begin{aligned} v(t) &= v_l(t) + v_{nl}(t), \\ v_l(t) &= \sum_{n=1}^{\infty} v_{bl}^n(t), \\ v_{nl}(t) &= \Gamma(\omega) \sum_{n=1}^{\infty} v_{nl}^1(t), \\ v_{bl}^n(t) &= \mathcal{F}^{-1}[E_n(\omega)C_{bl}(n\omega)], \\ v_{nl}^1(t) &= \sum_{n=1}^{\infty} \mathcal{F}^{-1}[E_{1n}(\omega)C_{nl}(n\omega)], \end{aligned} \quad (36)$$

where

$$\begin{aligned} E_{1n}(\omega) &= |E_1| \mathcal{F}^{-1}[\sin(n\omega t + n\angle E_1)], \\ \Delta_c^1(\omega) &= |\Delta_l(\omega)| \sin(\angle \Delta_l(\omega)), \\ \Gamma(\omega) &= 1 / (1 - \sum_{n=3}^{\infty} \Psi_n(\omega) \Delta_c^n(\omega) / \Delta_c^1(\omega)), \\ \Psi_n(\omega) &= |\mathcal{L}_{nl}(n\omega)| / |1 + \mathcal{L}_{bl}(n\omega)|, \quad n = 2k + 1, \quad k \in \mathbb{N}, \\ \Delta_c^n(\omega) &= -|\Delta_l(n\omega)| \sin(\angle \mathcal{L}_{nl}(n\omega) - \angle(1 + \mathcal{L}_{bl}(n\omega)) + \\ &\quad \angle \Delta_l(n\omega)), \quad \text{for } n > 1. \end{aligned} \quad (37)$$

Functions  $C_{bl}(\omega)$ ,  $C_{nl}(\omega)$ ,  $\Delta_l(n\omega)$ ,  $\mathcal{L}_{bl}(n\omega)$  and  $\mathcal{L}_{nl}(n\omega)$  can be found in (2), (24), (22) and (29), respectively.

*Proof.* The proof is provided in Appendix E.  $\square$

**Remark 2.** From (32) and (36),  $\Gamma(\omega)$  in (37) represents the ratio of  $v_{nl}(t) = 1 + \sum_{n=3}^{\infty} v_{nl}^n(t)$  to  $v_{nl}^1(t)$  at the input frequency  $\omega$ . It serves as an indicator of the relative magnitude of higher-order harmonics  $\sum_{n=3}^{\infty} v_{nl}^n(t)$  compared to the first-order harmonic  $v_{nl}^1(t)$ . A larger value of  $\Gamma(\omega)$  indicates a relatively larger magnitude of higher-order harmonics in closed-loop reset systems.

Building upon the analytical model introduced in Theorem 3, we propose a new Higher-Order Sinusoidal Input Describing Function (HOSIDF) for the frequency response analysis of closed-loop reset control systems. The detailed formulation is presented in Theorem 4.

**Theorem 4.** (The closed-loop HOSIDF for SISO reset control systems) Consider a closed-loop SISO reset control system in Fig. 1 with a reset controller  $C$  (1) (where  $n_r = 1$ ) and to a sinusoidal reference input signal  $r(t) = |R|\sin(\omega t)$ . This system complies with Assumptions 2 and 3. By employing the ‘‘Virtual Harmonics Generator’’ to the input signal  $r(t)$ , the signal  $r_n(t) = |R|\sin(n\omega t)$ ,  $n \in \mathbb{N}$  is introduced, along with its Fourier transform  $R_n(\omega)$ . The transfer functions  $\mathcal{S}_n(\omega)$ ,  $\mathcal{T}_n(\omega)$ , and  $C\mathcal{S}_n(\omega)$  of the closed-loop reset system at steady states are defined as follows:

$$\mathcal{S}_n(\omega) = \frac{E_n(\omega)}{R_n(\omega)} = \begin{cases} \frac{1}{1 + \mathcal{L}_o(\omega)}, & \text{for } n = 1 \\ -\frac{\Gamma(\omega)\mathcal{L}_{nl}(n\omega)\mathcal{S}_1(\omega)e^{jn\angle \mathcal{S}_1(\omega)}}{1 + \mathcal{L}_{bl}(n\omega)}, & \text{for odd } n > 1 \\ 0, & \text{for even } n \geq 2 \end{cases} \quad (38)$$

$$\mathcal{T}_n(\omega) = \frac{Y_n(\omega)}{R_n(\omega)} = \begin{cases} \frac{\mathcal{L}_o(\omega)}{1 + \mathcal{L}_o(\omega)}, & \text{for } n = 1 \\ \frac{\Gamma(\omega)\mathcal{L}_{nl}(n\omega)\mathcal{S}_1(\omega)e^{jn\angle \mathcal{S}_1(\omega)}}{1 + \mathcal{L}_{bl}(n\omega)}, & \text{for odd } n > 1 \\ 0, & \text{for even } n \geq 2 \end{cases} \quad (39)$$

$$C\mathcal{S}_n(\omega) = \frac{U_n(\omega)}{R_n(\omega)} = \frac{\mathcal{T}_n(\omega)}{\mathcal{P}(n\omega)}, \quad (40)$$

where

$$\begin{aligned} R_n(\omega) &= |R|\mathcal{F}[\sin(n\omega t)], \\ \mathcal{L}_o(n\omega) &= \mathcal{L}_{bl}(n\omega) + \Gamma(\omega)\mathcal{L}_{nl}(n\omega). \end{aligned} \quad (41)$$

Functions  $\mathcal{L}_{bl}(n\omega)$ ,  $\mathcal{L}_{nl}(n\omega)$ , and  $\Gamma(\omega)$  are given in (29) and (37).

*Proof.* The proof is provided in Appendix F.  $\square$

**Remark 3.** Consider a SISO reset control system under Assumptions 2 and with a sinusoidal reference signal  $r(t) = |R|\sin(\omega t)$ , as depicted in Fig. 1. By utilizing the “Virtual Harmonic Generator”, the input signal  $r(t)$  generates  $n = 2k + 1 (k \in \mathbb{N})$  harmonics  $r_n(t) = |R|\sin(n\omega t)$ . The Fourier transform for  $r_n(t)$  is denoted as  $R_n(\omega)$ . The steady-state error signal  $e(t)$ , output signal  $y(t)$ , and control input signal  $u(t)$  are expressed as follows:

$$\begin{aligned} e(t) &= \sum_{n=1}^{\infty} e_n(t) = \sum_{n=1}^{\infty} \mathcal{F}^{-1}[\mathcal{S}_n(\omega)R_n(\omega)], \\ y(t) &= \sum_{n=1}^{\infty} y_n(t) = \sum_{n=1}^{\infty} \mathcal{F}^{-1}[\mathcal{T}_n(\omega)R_n(\omega)], \\ u(t) &= \sum_{n=1}^{\infty} u_n(t) = \sum_{n=1}^{\infty} \mathcal{F}^{-1}[\mathcal{C}\mathcal{S}_n(\omega)R_n(\omega)]. \end{aligned} \quad (42)$$

**Remark 4.** The function  $\Gamma(\omega)$  in (37), represents the ratio of the nonlinear outputs  $v_{nl}(t)$  to  $v_{nl}^1(t)$  in (36) at input frequency  $\omega$ . Previous frequency response analysis methods, Method A and Method B, introduced in Section 2.4, assume that the higher-order harmonics  $v_{nl}^n(t)$  (for  $n > 1$ ) generated by  $e_n(t)$  are zero, thereby implying  $\Gamma(\omega) = 1$ . However, this assumption does not hold across the entire frequency spectrum of the reset control system, leading to inaccuracies in the analysis. Theorem 4 addresses these inaccuracies analytically by introducing  $\Gamma(\omega)$  in (37). While Theorem 4 exhibits comparable accuracy to Method B within the frequency range where  $\Gamma(\omega) = 1$ , it has superior accuracy compared to Method B when  $\Gamma(\omega) \neq 1$ , particularly in scenarios where the magnitudes of higher-order harmonics  $v_{nl}^n(t)$  (for  $n > 1$ ) are significant.

## 5. Case Study 1: Proportional-Clegg-Integrator Proportional-Integrator-Derivative (PCI-PID) Control System

In this section, we design a PCI-PID controller on a precision motion stage for validating the Theorem 4.

### 5.1. Precision Positioning Setup

The plant utilized in this study is a planar motion system with three degrees of freedom as depicted in

Fig. 6(a), referred to as “Spyder” stage. This system employs dual leaf flexures, each associated with corresponding masses ( $M_1$ ,  $M_2$ ,  $M_3$ ), for connection to the base ( $M_c$ ). These masses are driven by three voice coil actuators labeled  $A_1$ ,  $A_2$ , and  $A_3$ . Linear encoders (denoted as “Enc”), specifically Mercury M2000 with a resolution of 100 nm and sampled at 10 kHz, are utilized to monitor the positions of the masses. Additionally, with additional oversampling introduced on the FPGA, this resolution is increased to 3.125 nm. For the SISO investigation, only actuator  $A_1$  is used to position mass  $M_1$ . The control systems are implemented on an NI compactRIO platform and incorporate a linear current source power amplifier.

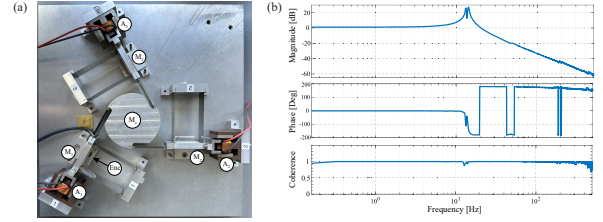


Figure 6: (a) The planar precision positioning system. (b) The FRF data from actuator  $A_1$  to attached mass  $M_1$ .

Figure 6(b) depicts the measured Frequency Response Function (FRF) of the system, which exhibits a collocated double mass-spring-damper system with additional high-frequency parasitic dynamics. To improve control clarity, the system is approximated to a single eigenmode mass-spring-damper system using Matlab’s identification tool. The transfer function of the system is expressed as:

$$\mathcal{P}(s) = \frac{6.615e5}{83.57s^2 + 279.4s + 5.837e5}. \quad (43)$$

### 5.2. The Validation and the Limitation of Theorem 4 on the Analysis of the PCI-PID Control System

The PID controller is widely used in industries. Within the PID framework, we design a PCI-PID controller for the precision motion stage, as shown in Fig. 7. The parameters of the PCI-PID system are as follows: the reset value  $\gamma = 0$ ,  $K_p = 20.5$ , the cut-off frequency  $\omega_c = 2\pi \cdot 150$  [rad/s],  $\omega_d = \omega_c/4.8$ ,  $\omega_t = \omega_c \cdot 4.8$ ,  $\omega_f = 10\omega_c$ , and  $\omega_i = 0.1\omega_c$ . The design specifications for the PCI-PID system aim to achieve a bandwidth (BW) of 150 Hz and a phase margin (PM) of 50° in the open-loop. Additionally, the stability and convergence of the system have been verified through testing.

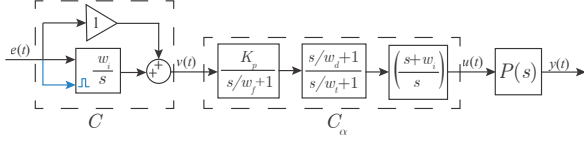


Figure 7: The open-loop block diagram of the PCI-PID control system.

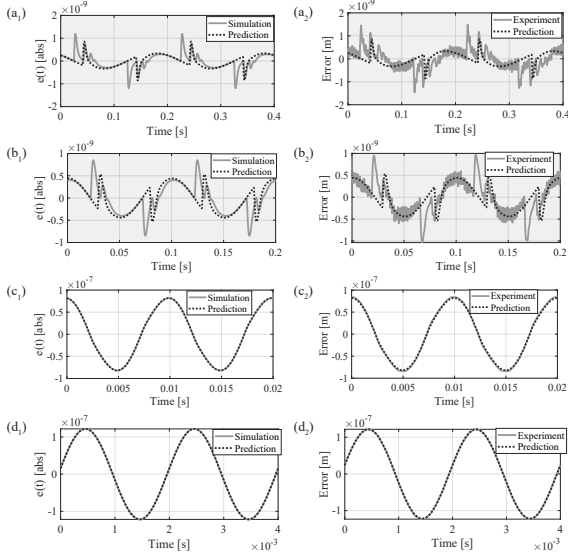


Figure 8: The steady-state errors  $e(t)$  for the PCI-PID system under sinusoidal input  $r(t) = \sin(2\pi ft)$  at input frequencies  $f$  of 5 Hz in  $(a_1)$  and  $(a_2)$ , 10 Hz in  $(b_1)$  and  $(b_2)$ , 100 Hz in  $(c_1)$  and  $(c_2)$ , and 500 Hz in  $(d_1)$  and  $(d_2)$  as predicted, simulated, and experimentally measured. The grey background indicates scenarios involving multiple-reset actions.

The steady-state errors indicate the tracking precision of the motion control system. We utilize the steady-state errors to validate the accuracy of Theorem 4. Figures 8 $(c_1)$ ,  $(c_2)$ ,  $(d_1)$ , and  $(d_2)$  depict the steady-state errors  $e(t)$  of the PCI-PID system under input signal  $r(t) = 1E - 7 \sin(2\pi ft)$  at input frequencies  $f$  of 100 Hz and 500 Hz, as predicted, simulated, and measured in experiments. The alignment between the predictions, simulations, and experiments suggests that Theorem 4 accurately predicts the system behavior. Note that the reference input signal used in the experiments is  $r(t) = 1E - 7 \sin(2\pi ft)$  [m].

However, as depicted in Fig. 8 $(a_1)$ ,  $(a_2)$ ,  $(b_1)$ , and  $(b_2)$ , at input frequencies of 5 Hz and 10 Hz where multiple resets per cycle occur, Assumption 3 is not satisfied. This results in inaccuracies in the predictions provided by Theorem 4. Note that the jagged noises observed in the measured signals during experiments arise from the sensor's resolution limitations. In prac-

tical scenarios, multiple resets can introduce excessive nonlinearity to the system, leading to undesired performance issues such as the limit cycle problem in the PI+CI system Baños et al. (2011). It is preferred to design reset systems without multiple resets across the entire frequency range. The examples of the PCI-PID system in Fig. 8 $(a_1)$ - $(b_2)$  serve to illustrate the limitation of the accuracy of the new analysis method imposed by Assumption 3.

In Section 6, we introduce a new reset control structure as a case study aimed at addressing the multiple-reset limitation observed in the PCI-PID control structure. This new structure is designed to achieve two reset instants per steady-state cycle, thereby satisfying Assumption 3 required for Theorem 4.

## 6. Case Study 2: Two-reset-PCI-PID (T-PCI-PID) Control System

### 6.1. The Two-Reset Control System

In this section, we introduced a new reset control structure termed the Two-Reset Control System (T-RCS), illustrated in Fig. 9. This structure forces the system to reset twice per steady-state cycle under a sinusoidal reference input signal, serving as an illustrative example for validating Theorem 4.

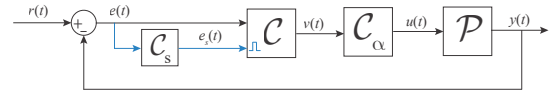


Figure 9: Block diagram of the T-reset system, where  $C_s(s)$  is given in (44) and  $e_s(t)$  is the reset signal.

In a traditional closed-loop reset system under sinusoidal input  $r(t) = |R|\sin(\omega t)$ , the error signal  $e(t)$  is nonlinear and includes infinitely many harmonics  $e_n(t)$  as defined in (13). This new T-RCS introduces a transfer function  $C_s$  between the error signal  $e(t)$  and the reset-triggered signal  $e_s(t)$ . The transfer function of  $C_s(s)$  is given by

$$C_s(s) = k_{cs} \left[ \frac{(s/(\omega))^2 + s/(\omega \cdot Q_1) + 1}{(s/(\omega))^2 + s/(\omega \cdot Q_2) + 1} \right], \quad (44)$$

where  $Q_1 < Q_2 \in \mathbb{R}^+$ . In this paper, we set  $Q_1 = 1$ ,  $Q_2 = 100$ , and  $k_{cs} = 0.05$ .

From (44),  $C_s(s)$  functions as an anti-notch filter. This filter allows frequencies within a specific range to pass through while attenuating all others. By adjusting the parameters  $Q_1$  and  $Q_2$ , the frequency range of interest can be tailored. For example, selecting  $Q_1 =$

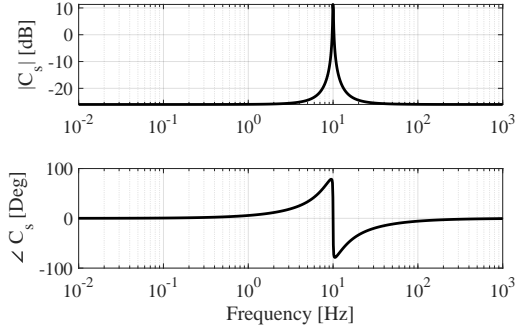


Figure 10: Bode Plot of  $C_s(s)$  for  $\omega = 2\pi \cdot 10$  [rad/s].

1,  $Q_2 = 100$ ,  $k_{cs} = 0.05$  for a frequency of  $\omega = 2\pi \cdot 10$  [rad/s] yields the Bode plot depicted in Fig. 10. At the frequency  $\omega = 2\pi \cdot 10$  [rad/s],  $\angle C_s(\omega) = 0$ , and the magnitude  $|C_s(\omega)|$  is relatively a peak to other frequencies. Therefore,  $C_s(s)$  approximately allows signals with a frequency of  $\omega$  to pass through. By aligning  $\omega$  with the first-order input frequency in  $e(t)$  (13), the reset-triggered signal  $e_s(t)$  is approximately expressed as:

$$e_s(t) = |E_1 C_s| \sin(\omega t + \angle E_1). \quad (45)$$

From (45), the reset-triggered signal  $e_s(t)$  shares the same frequency and phase as the first-order harmonic  $e_1(t)$  in the error signal  $e(t)$ . Since the reset-triggered signal  $e_s(t)$  is phase-dependent and amplitude-independent, equation (45) indicates that the reset action of  $C$  is triggered based on  $e_1(t)$ . Thus, within this structure, the T-RCS ensures two reset instants per steady-state. This example serves to validate Theorem 4, satisfying Assumption 3.

## 6.2. The Application of Theorem 4 to Analyze the T-PCI-PID System

### 6.2.1. The Accuracy of Theorem 4

Figure 11 shows the structure of the Two-reset-PCI PID (T-PCI-PID) Control System. The transfer function  $C_s$  is defined in (44). Except for the setting for shaping filter  $C_s$  with  $Q_1 = 1$ ,  $Q_2 = 100$ ,  $K_{cs} = 0.05$ , the parameters of the T-PCI-PID system are specified the same as those of the PCI-PID control system in Case Study 1. It has been verified that the T-PCI-PID system is stable and convergent.

Figure 12 (a<sub>1</sub>)-(d<sub>1</sub>) illustrates the simulated and Theorem 4-predicted steady-state errors  $e(t)$  for the T-PCI-PID system. These simulations consider a reference input signal  $r(t) = 1E - 7 \sin(2\pi ft)$  at frequencies  $f$  of 5 Hz, 10 Hz, 100 Hz, and 500 Hz. Given that the reset action is amplitude-independent, we display the scaled

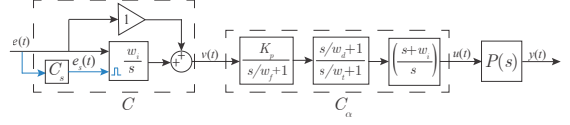


Figure 11: The open-loop block diagram of the T-PCI-PID control system.

reset triggered signals for these frequencies. The reset triggered signal  $e_s(t)$  forces two reset instants per steady-state period in multiple-reset systems at input frequencies 5 Hz and 10 Hz, while it maintains the reset instants unchanged in two-reset systems at input frequencies 100 Hz and 500 Hz.

The analytical predictions closely align with the simulations in T-PCI-PID systems, validating the accuracy of Theorem 4. This conclusion is further supported by the experimental results in Fig. 12 (a<sub>2</sub>)-(d<sub>2</sub>). Note that the jagged signal observed at input frequencies 5 Hz and 10 Hz in the measured results arises from sensor limitations.

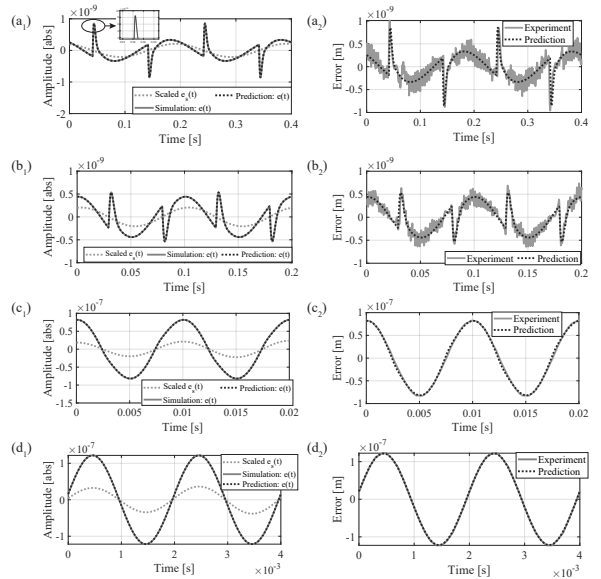


Figure 12: The steady-state error  $e(t)$  for the T-PCI-PID system under sinusoidal input  $r(t) = \sin(2\pi ft)$  at input frequencies  $f$  of 5 Hz in (a<sub>1</sub>) and (a<sub>2</sub>), 10 Hz in (b<sub>1</sub>) and (b<sub>2</sub>), 100 Hz in (c<sub>1</sub>) and (c<sub>2</sub>), and 500 Hz in (d<sub>1</sub>) and (d<sub>2</sub>) as predicted, simulated, and experimentally measured.  $e_s(t)$  represents the reset triggered signal.

Experimental results presented in Fig. 12 not only validate the accuracy of Theorem 4 but also demonstrate the superior performance achieved by the T-PCI-PID system compared to the PCI-PID under sinusoidal inputs. The T-PCI-PID system effectively reduces low-frequency steady-state error while retaining

high-frequency performance. For instance, under the same input signal at the input frequency of 10 Hz, the T-PCI-PID system in Fig. 12(b<sub>2</sub>) has a maximum steady-state error magnitude of 0.5E-9 [m], while the PCI-PID system in Fig. 8(b<sub>2</sub>) has a maximum steady-state error magnitude of 1E-9 [m]. However, since this paper primarily focuses on developing frequency response analysis for closed-loop reset systems, a comprehensive exploration of the T-RCS structure's capabilities across diverse situations will be addressed in future research.

### 6.2.2. The Relation of the Accuracy of Theorem 4 and the Number of Harmonics

Let  $e_{\text{sim}}(t)$  and  $e_{\text{pre}}(t)$  denote the simulated and predicted steady-state errors in the T-PCI-PID system, respectively. The Prediction Error (PE) between them is defined as  $\text{PE} = |e_{\text{sim}}(t) - e_{\text{pre}}(t)|$ .

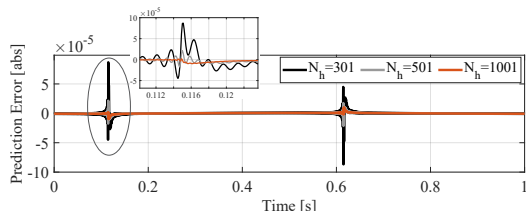


Figure 13: The PE of the T-PCI-PID control system under the input  $r(t) = \sin(2\pi t)$  for different numbers of harmonics ( $N_h$ ) included in the prediction calculation process, specifically 301, 501, and 1001.

Figure 13 shows the relationship between the PE and the number of harmonics (denoted as  $N_h$ ) included in the prediction calculation process, in the T-PCI-PID control system under a sinusoidal input signal  $r(t) = \sin(2\pi t)$ . As the number of harmonics  $N_h$  increases, the accuracy of the method increases. Ideally, PE approaches 0 as  $N_h$  tends to infinity. The zoom-in plot emphasizes the differences in predictions between the simulation and Theorem 4, resembling vibration signals. This discrepancy arises because Theorem 4 calculates outputs by summing a finite number of sinusoidal harmonics. The unaccounted infinite harmonics contribute to the prediction error, resulting in a pattern reminiscent of vibrations. There is a trade-off between the PE and  $N_h$  (indicating the calculation time in practice). Readers can strive to minimize PE while considering the computational time trade-off.

### 6.3. Discussion: The Usability of Theorem 4 in the Reset Systems Design

In linear systems, the analytical connection between open-loop and closed-loop frequency-domain analysis

serves as an effective tool for designing and predicting the performance of the systems. Let  $\mathcal{L}_n(\omega)$  and  $\mathcal{S}_n(\omega)$  represent the open-loop transfer function and the closed-loop sensitivity function, respectively. However, in reset systems, the relationship  $\mathcal{S}_n(\omega) = 1/(\mathcal{L}_n(\omega) + 1)$  does not hold, neither for the first-order harmonic (for  $n = 1$ ) nor higher-order harmonics (for  $n > 1$ ). The developed closed-loop sensitivity functions in (38) illustrate that the first and higher-order harmonics in the open-loop have a cross effect on the first and higher-order harmonics in the closed-loop, mediated by the parameter  $\Gamma(\omega)$ .

As highlighted in Remark 4, Method A and Method B assume  $\Gamma(\omega) = 1$  for all  $\omega$ , which implies that higher-order harmonics  $e_n(t)$  for  $n > 1$  undergo no reset actions, leading to inaccuracies. Theorem 4 addresses this issue by introducing the parameter  $\Gamma(\omega)$ . The parameter  $\Gamma(\omega)$  affects computations for both first-order and higher-order harmonics, as demonstrated in equations (38) to (41). Its introduction provides a more accurate representation of the system's behavior, particularly in scenarios involving significant higher-order harmonics. Moreover,  $\Gamma(\omega)$  can be used to design and tune reset systems to be less affected by higher-order harmonics, for improving system performance.

Figure 14 illustrates the  $\Gamma(\omega)$  values in the T-PCI-PID system when subjected to sinusoidal inputs across frequencies ranging from 1 Hz to 1000 Hz. It is evident from the figure that  $\Gamma(\omega) = 1$  does not hold across the entire frequency range. Given this context, comparing the new method with previous Methods A and B would be redundant, as these methods have already been shown to make inaccurate assumptions. To validate the accuracy of the new theorem, we directly compare its predictions with simulations and experiments in Section 6.2.1.

Note that the depiction of  $\Gamma(\omega)$  in Fig. 14 specifically pertains to the system described in case study 2. For different reset control systems,  $\Gamma(\omega)$  will vary as determined by (37).

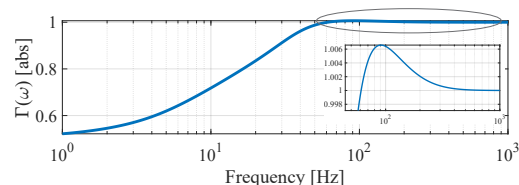


Figure 14: The  $\Gamma(\omega)$  of the T-PCI-PID control system.

Theorem 4 serves two primary purposes in the design of reset systems:

- (1) Assessing the time-domain performance of the closed-loop system, for example evaluating its tracking precision at various frequencies, as demonstrated in Fig. 8 and 12.
- (2) Analyzing the frequency-domain characteristics of closed-loop reset systems by generating plots of the closed-loop HOSIDF using (38) to (40), as exemplified in Fig. 15.

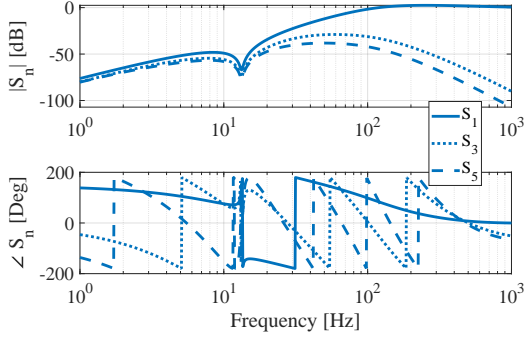


Figure 15: The Bode plot of the closed-loop Higher Order Sinusoidal Input Sensitivity Function (HOSISF)  $S_n(\omega)$  for the closed-loop T-PCI-PID control system, with the first three harmonics  $S_1$ ,  $S_3$ , and  $S_5$ .

Theorems 1, 2, 3, and 4 collectively offer tools to analyze the behavior of reset controllers in both open-loop and closed-loop, facilitating the application of loop-shaping techniques in the reset systems design in the future.

## 7. Conclusion

Reset control systems are effective in improving the performance of motion systems. To facilitate the practical design of reset systems, this study develops frequency response analysis methods for open-loop and closed-loop reset control systems, by assessing their steady-state responses to sinusoidal inputs. Results show the efficacy of the methods in predicting the precision of two-reset systems on precision motion stages. Moreover, the methods establish connections between open-loop and closed-loop analysis of reset systems. However, the paper primarily develops these analysis tools. Future research can explore practical applications of these frequency response analysis methods in designing reset control systems.

The frequency response analysis for closed-loop reset systems under sinusoidal disturbance and noise follows a similar derivation process as the theories presented in this paper. However, to emphasize and clarify the contribution of this paper, we have chosen not to include

analysis for systems with disturbance or noise inputs here. Instead, we plan to address these aspects in our future research discussing disturbances.

The frequency response analysis is currently limited to two-reset systems. In our future research, we aim to develop techniques to identify two-reset systems and analyze multiple-reset systems, thereby expanding the scope of our analysis methods. Furthermore, the newly introduced Two-Reset Control System (T-RCS) in this research is designed to enforce two reset instants per steady-state cycle when the system is subjected to sinusoidal inputs. The T-RCS has shown improved steady-state tracking precision at low frequencies compared to traditional reset systems under sinusoidal reference inputs. The enhanced performance is attributed to the elimination of multiple-reset occurrences achieved by the T-RCS. The practical application of the T-RCS under various types of inputs are worth exploring in future research endeavors.

## Appendix A. Proof for Lemma 1

*Proof.* Consider a GCI subjected to a sinusoidal input signal  $e(t) = |E_1|\sin(\omega t)$ , under Assumption 1 and the Zero-free condition in (8), at steady states.

Based on (1), the output signal  $u_{ci}(t)$  of the GCI (with  $A_R = 0, B_R = 1, C_R = 1, D_R = 0$ ) is given by

$$\begin{cases} \dot{u}_{ci}(t) = e(t), & e(t) \neq 0, \\ u_{ci}(t^+) = \gamma u_{ci}(t), & e(t) = 0. \end{cases} \quad (\text{A.1})$$

For its BLS (which is an integrator), we have

$$\dot{u}_i(t) = e(t). \quad (\text{A.2})$$

Define  $q_i(t) = u_{ci}(t) - u_i(t)$ . From (A.1) and (A.2), we have

$$\begin{cases} \dot{q}_i(t) = \dot{u}_{ci}(t) - \dot{u}_i(t) = 0, & e(t) \neq 0, \\ q_i(t^+) = \gamma q_i(t) + (\gamma - 1)u_i(t), & e(t) = 0. \end{cases} \quad (\text{A.3})$$

The reset instant of the GCI with a sinusoidal input signal  $e(t) = |E_1|\sin(\omega t)$  is determined by  $t_i = i\pi/\omega$ , where  $i \in \mathbb{Z}^+$  and  $e(t_i) = 0$ . Utilizing (A.3), the signal  $q_i(t)$  between two consecutive reset instants  $[t_i^+, t_{i+1}]$  (where  $t_i^+$  denotes the after-reset instant) is expressed as:

$$q_i(t) = q_i(t_i^+) + \int_{t_i^+}^t \dot{q}_i(\tau) d\tau = q_i(t_i^+), \quad t \in [t_i^+, t_{i+1}]. \quad (\text{A.4})$$

Given the input signal  $e(t) = |E_1|\sin(\omega t)$  and based on the state-space equation in (1), at the reset instant  $t_i =$

$i\pi/\omega$ , the base-linear output  $u_i(t_i)$  is given by:

$$u_i(t_i) = \begin{cases} 0, & \text{for even } i, \\ 2|E_1|/\omega, & \text{for odd } i. \end{cases} \quad (\text{A.5})$$

Combining (A.3), (A.4), and (A.5), at the reset instant  $t_i$ ,  $q_i(t_i^+)$  is given by

$$\begin{aligned} q_i(t_i^+) &= \gamma q_i(t_{i-1}^+) + (\gamma - 1)u_i(t_i) \\ &= \begin{cases} \gamma q_i(t_{i-1}^+), & \text{for even } i, \\ \gamma q_i(t_{i-1}^+) + 2|E_1|(\gamma - 1)/\omega, & \text{for odd } i. \end{cases} \end{aligned} \quad (\text{A.6})$$

Based on (A.6), for an odd  $i$ ,  $q_i(t_i^+)$  is given by

$$\begin{aligned} q_i(t_i^+) &= q_i(t_{i+2}^+) \\ &= \gamma q_i(t_{i+1}^+) + 2|E_1|(\gamma - 1)/\omega \\ &= \gamma^2 q_i(t_i^+) + 2|E_1|(\gamma - 1)/\omega. \end{aligned} \quad (\text{A.7})$$

Equations (A.6) and (A.7) can be concluded that

$$q_i(t_i^+) = \begin{cases} -2|E_1|\gamma(\gamma + 1)^{-1}/\omega, & \text{for even } i, \\ -2|E_1|(\gamma + 1)^{-1}/\omega, & \text{for odd } i. \end{cases} \quad (\text{A.8})$$

Combining (A.4) and (A.8),  $q_i(t)$  in the time domain can be derived as follows:

$$q_i(t) = \begin{cases} -2|E_1|\gamma(\gamma + 1)^{-1}/\omega, & \text{for } t \in [2k, 2k + 1) \cdot \pi/\omega, \\ -2|E_1|(\gamma + 1)^{-1}/\omega, & \text{for } t \in [2k + 1, 2k + 2) \cdot \pi/\omega. \end{cases} \quad (\text{A.9})$$

Here we conclude the proof.  $\square$

## Appendix B. Proof for Theorem 1

*Proof.* Consider a reset controller  $C$  (1) where  $n_r = 1$  with an input signal of  $e(t) = |E_n|\sin(n\omega t + \angle E_n)$  ( $\angle E_s \in (-\pi, \pi)$ ,  $n = 2k + 1$ ,  $k \in \mathbb{N}$ ) and a reset triggered signal of  $e_s(t) = |E_s|\sin(\omega t + \angle E_s)$  ( $\angle E_s \in (-\pi, \pi)$ ), at steady states. Let  $x_c(t)$  and  $x_{bl}(t)$  denote the state and the base-linear state of the  $C$  and the BLC  $C_{bl}$ , respectively. Define

$$x_{nl}(t) = x_c(t) - x_{bl}(t) \in \mathbb{R}^{n_c \times 1}, \quad (\text{B.1})$$

where  $n_c$  is the number of states of the reset controller  $C$  and  $x_{bl}(t)$  is given by

$$x_{bl}(t) = |E_n \Delta_l(n\omega)| \sin(n\omega t + \angle E_n + \angle \Delta_l(n\omega)), \quad (\text{B.2})$$

where

$$\Delta_l(n\omega) = (jn\omega I - A_R)^{-1} B_R \in \mathbb{R}^{n_c \times 1}. \quad (\text{B.3})$$

Based on (1) and (B.1), we have:

$$\begin{cases} \dot{x}_{nl}(t) = A_R x_{nl}(t), & e_s(t) \neq 0, \\ x_{nl}(t^+) = A_\rho x_{nl}(t) + (A_\rho - I)x_{bl}(t), & e_s(t) = 0. \end{cases} \quad (\text{B.4})$$

For the reset controller  $C$  with a reset triggered signal of  $e_s(t) = |E_s|\sin(\omega t + \angle E_s)$ , the set of reset instants is denoted by  $J_o := \{t_i \mid t_i = (i\pi - \angle E_s)/\omega, i \in \mathbb{Z}^+\}$ . The reset interval is given by  $\sigma_i = t_{i+1} - t_i = \pi/\omega$ . According to (B.4), between two consecutive reset instants  $[t_i^+, t_{i+1}]$  where  $e_s(t) \neq 0$ , the expression for  $x_{nl}(t)$  is given by

$$x_{nl}(t) = e^{A_R(t-t_i)} \Delta_n(\omega), \quad \text{for } t \in [t_i^+, t_{i+1}], \quad (\text{B.5})$$

where  $\Delta_n(\omega) \in \mathbb{R}^{n_c \times 1}$  is a constant matrix independent of time  $t$ .

Based on (B.5), at the reset instant  $t_{i+1} \in J_o$ ,  $x_{nl}(t_{i+1})$  is given by

$$x_{nl}(t_{i+1}) = e^{A_R(t_{i+1}-t_i)} \Delta_n(\omega) = e^{A_R \pi/\omega} \Delta_n(\omega). \quad (\text{B.6})$$

From (B.4),  $x_{nl}(t^+)$  at the reset instant  $t_{i+1}$  is given by

$$x_{nl}(t_{i+1}^+) = A_\rho x_{nl}(t_{i+1}) + (A_\rho - I)x_{bl}(t_{i+1}). \quad (\text{B.7})$$

Substituting  $x_{nl}(t_{i+1})$  from (B.6) into (B.7),  $x_{nl}(t_{i+1}^+)$  is obtained as

$$x_{nl}(t_{i+1}^+) = A_\rho e^{A_R \pi/\omega} \Delta_n(\omega) + (A_\rho - I)x_{bl}(t_{i+1}). \quad (\text{B.8})$$

From (B.2), at the reset instant  $t_i = (i\pi - \angle E_s)/\omega$ , the base-linear state is given by

$$\begin{aligned} x_{bl}(t_i) &= |E_n \Delta_l(n\omega)| \sin(ni\pi + \angle E_n + \angle \Delta_l(n\omega) - n\angle E_s) \\ &= \begin{cases} |E_n \Delta_l(n\omega)| \sin(\angle \Delta_l(n\omega) + \angle E_n - n\angle E_s), & \text{for even } i, \\ -|E_n \Delta_l(n\omega)| \sin(\angle \Delta_l(n\omega) + \angle E_n - n\angle E_s), & \text{for odd } i, \end{cases} \end{aligned} \quad (\text{B.9})$$

where  $\Delta_l(n\omega)$  is given in (B.3).

Define

$$\Delta_c^n(\omega) = |\Delta_l(n\omega)| \sin(\angle \Delta_l(n\omega) + \angle E_n - n\angle E_s) \in \mathbb{R}^{n_c \times 1}, \quad (\text{B.10})$$

and substitute  $\Delta_c^n(\omega)$  from (B.10) into (B.9), we have

$$x_{bl}(t_i) = \begin{cases} |E_n| \Delta_c^n(\omega), & \text{for even } i, \\ -|E_n| \Delta_c^n(\omega), & \text{for odd } i. \end{cases} \quad (\text{B.11})$$

From (B.11), at the reset instant  $t_{i+1} = ((i+1)\pi - \angle E_s)/\omega$ , the expression for  $x_{bl}(t_{i+1})$  is written as:

$$x_{bl}(t_{i+1}) = \begin{cases} -|E_n| \Delta_c^n(\omega), & \text{for even } i, \\ |E_n| \Delta_c^n(\omega), & \text{for odd } i, \end{cases} \quad (\text{B.12})$$

Substituting  $x_{bl}(t_{i+1})$  from (B.12) into (B.8),  $x_{nl}(t_{i+1}^+)$  is derived as

$$x_{nl}(t_{i+1}^+) = \begin{cases} A_\rho e^{A_R \pi / \omega} \Delta_n(\omega) - (A_\rho - I) |E_n| \Delta_c^n(\omega), & \text{for even } i, \\ A_\rho e^{A_R \pi / \omega} \Delta_n(\omega) + (A_\rho - I) |E_n| \Delta_c^n(\omega), & \text{for odd } i. \end{cases} \quad (\text{B.13})$$

From (B.13), we have

$$x_{nl}(t_i^+) = \begin{cases} A_\rho e^{A_R \pi / \omega} \Delta_n(\omega) + (A_\rho - I) |E_n| \Delta_c^n(\omega), & \text{for even } i, \\ A_\rho e^{A_R \pi / \omega} \Delta_n(\omega) - (A_\rho - I) |E_n| \Delta_c^n(\omega), & \text{for odd } i. \end{cases} \quad (\text{B.14})$$

From (B.5), at the reset instant  $t_i^+$ , we have

$$x_{nl}(t_i^+) = \Delta_n(\omega). \quad (\text{B.15})$$

Let equations (B.14) and (B.15) be set equal to each other. Then,  $\Delta_n(\omega)$  is derived as follows:

$$\Delta_n(\omega) = \begin{cases} |E_n| \Delta_v^n(\omega), & \text{for even } i, \\ -|E_n| \Delta_v^n(\omega), & \text{for odd } i, \end{cases} \quad (\text{B.16})$$

where

$$\Delta_v^n(\omega) = (A_\rho e^{A_R \pi / \omega} - I)^{-1} (I - A_\rho) \Delta_c^n(\omega) \in \mathbb{R}^{n_c \times 1}. \quad (\text{B.17})$$

Since the reset interval  $\sigma_i = \pi/\omega$ , equations (B.5) and (B.16) together illustrate that  $x_{nl}(t)$  is bounded and has the same period  $2\pi/\omega$  as the reset triggered signal  $e_s(t)$ . The absolute integrability of  $x_{nl}(t)$  implies the existence of its Fourier and Laplace transforms. Let  $X_{nl}(s)$  denote the Laplace transform of  $x_{nl}(t)$ . From (B.5), for  $t \in [t_i^+, t_{i+1}]$ , the Laplace transform of  $x_{nl}(t)$  is expressed as:

$$X_{nl}(s) = \mathcal{L}[x_{nl}(t)] = (sI - A_R)^{-1} e^{-A_R t_i} \Delta_n(\omega). \quad (\text{B.18})$$

Define a parameter  $Q(s) = \mathcal{L}[q(t)]$  as:

$$Q(s) = (sI)^{-1} (sI - A_R) X_{nl}(s). \quad (\text{B.19})$$

Then, based on (B.18) and (B.19), for  $t \in [t_i^+, t_{i+1}]$ ,  $Q(s)$  is given by

$$Q(s) = (sI)^{-1} e^{-A_R t_i} \Delta_n(\omega). \quad (\text{B.20})$$

From (B.16) and (B.20), during the time interval  $[t_i^+, t_{i+1}]$ , the inverse Laplace transform of  $Q(s)$  is given by:

$$q(t) = \mathcal{L}^{-1}[Q(s)] = \begin{cases} |E_n| \Delta_v^n(\omega) u(t - t_i) + C_{\beta 1}, & \text{for even } i, \\ -|E_n| \Delta_v^n(\omega) u(t - t_i) + C_{\beta 2}, & \text{for odd } i, \end{cases} \quad (\text{B.21})$$

where  $u(t)$  is a unit step signal. The parameters  $C_{\beta 1} \in \mathbb{R}^{n_c \times 1}$  and  $C_{\beta 2} \in \mathbb{R}^{n_c \times 1}$  are the values of  $q(t)$  at the reset

instant  $t_i$ . From (B.21), we obtain that  $q(t)$  remains a constant matrix during the time interval  $[t_i^+, t_{i+1}]$ .

From (B.5), at the time instant  $t_{i+1}$ ,  $x_{nl}(t_{i+1}) = e^{A_R \pi / \omega} \Delta_n(\omega)$ . From (B.16),  $x_{nl}(t_i)$  is given by

$$x_{nl}(t_i) = \begin{cases} -|E_n| e^{A_R \pi / \omega} \Delta_v^n(\omega), & \text{for even } i, \\ |E_n| e^{A_R \pi / \omega} \Delta_v^n(\omega), & \text{for odd } i, \end{cases} \quad (\text{B.22})$$

From (B.5) and (B.16), at the time instant  $t_i^+$ ,  $x_{nl}(t_i^+)$  is given by

$$x_{nl}(t_i^+) = \begin{cases} |E_n| \Delta_v^n(\omega), & \text{for even } i, \\ -|E_n| \Delta_v^n(\omega), & \text{for odd } i. \end{cases} \quad (\text{B.23})$$

From the time instant  $t_i$  to  $t_i^+$ ,  $x_{nl}(t_i)$  jumps to  $x_{nl}(t_i^+)$ . From (B.22) and (B.23), this jump is given by

$$x_{nl}(t_i^+) - x_{nl}(t_i) = \begin{cases} |E_n| (I + e^{A_R \pi / \omega}) \Delta_v^n(\omega), & \text{for even } i, \\ -|E_n| (I + e^{A_R \pi / \omega}) \Delta_v^n(\omega), & \text{for odd } i. \end{cases} \quad (\text{B.24})$$

Substituting  $\Delta_v^n(\omega)$  from (B.17) into (B.24), we have

$$x_{nl}(t_i^+) - x_{nl}(t_i) = \begin{cases} |E_n| (I + e^{A_R \pi / \omega}) (A_\rho e^{A_R \pi / \omega} - I)^{-1} (I - A_\rho) \Delta_c^n(\omega), & \text{for even } i, \\ -|E_n| (I + e^{A_R \pi / \omega}) (A_\rho e^{A_R \pi / \omega} - I)^{-1} (I - A_\rho) \Delta_c^n(\omega), & \text{for odd } i. \end{cases} \quad (\text{B.25})$$

Define

$$\Delta_q^n(\omega) = (I + e^{A_R \pi / \omega}) (A_\rho e^{A_R \pi / \omega} - I)^{-1} (I - A_\rho) \Delta_c^n(\omega) \in \mathbb{R}^{n_c \times 1} \quad (\text{B.26})$$

and substitute  $\Delta_q^n(\omega)$  from (B.26) into (B.25), we have

$$x_{nl}(t_i^+) - x_{nl}(t_i) = \begin{cases} |E_n| \Delta_q^n(\omega), & \text{for even } i, \\ -|E_n| \Delta_q^n(\omega), & \text{for odd } i. \end{cases} \quad (\text{B.27})$$

This jump indicates that from the time instant  $t_i$  to  $t_i^+$ ,  $x_{nl}(t)$  is an impulse signal denoted by  $\zeta_{nl}(t)$ . From (B.27),  $\zeta_{nl}(t)$  is expressed as:

$$\zeta_{nl}(t) = [x_{nl}(t_i^+) - x_{nl}(t_i)] \delta(t - t_i) = \begin{cases} |E_n| \Delta_q^n(\omega) \delta(t - t_i), & \text{for even } i, \\ -|E_n| \Delta_q^n(\omega) \delta(t - t_i), & \text{for odd } i, \end{cases} \quad (\text{B.28})$$

where  $\delta(t)$  represents the Dirac delta function.

Since the Laplace transform of the delta function is 1, the Laplace transform of the impulse signal  $\zeta_{nl}(t)$  in (B.28) is given by:

$$\zeta_{nl}(s) = \begin{cases} |E_n| \Delta_q^n(\omega) e^{-t_i s}, & \text{for even } i, \\ -|E_n| \Delta_q^n(\omega) e^{-t_i s}, & \text{for odd } i. \end{cases} \quad (\text{B.29})$$

The impulse response is defined as the response of a system to a Dirac delta input [Pesaran and Shin \(1998\)](#).



Define a signal  $\zeta_q(t)$  as the impulse response of the impulse signal  $\zeta_{nl}(t)$  filtered through the linear time invariant (LTI) transfer function  $(sI)^{-1}(sI - A_R)$ . From (B.29),  $\zeta_q(t)$  is given by:

$$\begin{aligned}\zeta_q(t) &= \mathcal{L}^{-1}[(sI)^{-1}(sI - A_R)\zeta_{nl}(s)] \\ &= \begin{cases} |E_1|\Delta_q^n(\omega)\delta(t - t_i) - |E_n|A_R\Delta_q^n(\omega), & \text{for even } i, \\ -|E_1|\Delta_q^n(\omega)\delta(t - t_i) + |E_n|A_R\Delta_q^n(\omega), & \text{for odd } i. \end{cases} \end{aligned} \quad (\text{B.30})$$

Equation (B.30) demonstrates that at the time instant  $t_i$ ,  $\zeta_q(t_i)$  has an initial value of  $\pm|E_n|A_R\Delta_q^n(\omega)$  and undergoes a jump of:

$$\zeta_q(t_i^+) - \zeta_q(t_i) = \begin{cases} |E_n|\Delta_q^n(\omega), & \text{for even } i, \\ -|E_n|\Delta_q^n(\omega), & \text{for odd } i. \end{cases} \quad (\text{B.31})$$

From (B.19), the signal  $x_{nl}(t)$  filtered by  $(sI)^{-1}(sI - A_R)$  generates the signal  $q(t)$ . Equations (B.30) and (B.31) demonstrate that at the time instant  $t_i$  to  $t_i^+$ , the signal  $x_{nl}(t_i)$  jumps to  $x_{nl}(t_i^+)$ . The jump  $\zeta_{nl}(t)$ , filtered by the transfer function  $(sI)^{-1}(sI - A_R)$ , generates a jump  $\zeta_q(t_i^+) - \zeta_q(t_i)$  in (B.31). Thus, from (B.19), (B.30), and (B.31), the jump in  $q(t) = \mathcal{L}^{-1}[Q(s)]$  at the time instant  $t_i$  is given by:

$$q(t_i^+) - q(t_i) = \zeta_q(t_i^+) - \zeta_q(t_i). \quad (\text{B.32})$$

Based on (B.31) and (B.32), at the time instant  $t_i$ , we have

$$q(t_i^+) = \begin{cases} q(t_i) + |E_n|\Delta_q^n(\omega), & \text{for even } i, \\ q(t_i) - |E_n|\Delta_q^n(\omega), & \text{for odd } i. \end{cases} \quad (\text{B.33})$$

From (B.21),  $q(t_i^+)$  for even  $i$  is given by

$$q(t_i^+) = |E_n|\Delta_v^n(\omega) + C_{\beta 1}. \quad (\text{B.34})$$

From (B.33), at the time instant  $t_i$  for even  $i$ ,  $q(t_i^+) = q(t_i) + |E_n|\Delta_q^n(\omega)$ . Then, based on (B.21) and (B.33),  $q(t_i^+)$  for even  $i$  can be written as

$$q(t_i^+) = -|E_n|\Delta_v^n(\omega) + C_{\beta 2} + |E_n|\Delta_q^n(\omega). \quad (\text{B.35})$$

By setting equations (B.34) and (B.35) equal to each other, we get:

$$C_{\beta 1} = C_{\beta 2} - 2|E_n|\Delta_v^n(\omega) + |E_n|\Delta_q^n(\omega). \quad (\text{B.36})$$

Substituting  $C_{\beta 1}$  from (B.36) to (B.21),  $q(t)$  is given by

$$q(t) = \begin{cases} -|E_n|\Delta_v^n(\omega)u(t - t_{2k}) + |E_n|\Delta_q^n(\omega) + C_{\beta 2}, & \text{for } t \in [t_{2k}^+, t_{2k+1}], \\ -|E_n|\Delta_v^n(\omega)u(t - t_{2k+1}) + C_{\beta 2}, & \text{for } t \in [t_{2k+1}^+, t_{2k+2}], \end{cases} \quad (\text{B.37})$$

where  $k \in \mathbb{N}$ .

Let  $f(t)_k$  ( $k \in \mathbb{Z}^+$ ) represent the  $k$ -th state of a function  $f(t)$ . Considering the reset controller  $C$  (1) with resetting the first state where  $n_r = 1$ , the first state  $x_c(t_i)_1$  in the state  $x_c(t_i)$  is reset to  $\gamma x_c(t_i)_1$ , and there are no reset actions in state  $x_c(t)_k$  for  $k > 1$ . Therefore, we have

$$x_c(t)_k = x_{bl}(t)_k, \text{ for } k > 1. \quad (\text{B.38})$$

From (B.1), (B.28), and (B.38), we have

$$\begin{aligned}x_{nl}(t)_k &= 0, \text{ for } k > 1, \\ \Delta_q^n(\omega)_k &= 0, \text{ for } k > 1. \end{aligned} \quad (\text{B.39})$$

From (B.19) and (B.39), we have

$$q(t)_k = 0, \text{ for } k > 1. \quad (\text{B.40})$$

Equation (B.37) indicates that during the time interval  $[t_i^+, t_{i+1}]$ ,  $q(t)$  is a constant matrix. Equation (B.33) demonstrates that at the time instant  $t_i \in J_o$ ,  $q(t)$  has a jump of  $\pm|E_n|\Delta_q^n(\omega)$ . Therefore, the signal  $q(t)$  is absolutely integrable, ensuring the existence of its Fourier and Laplace transforms. Since  $\sigma_i = t_{i+1} - t_i = \pi/\omega$ , from (B.33), (B.37), and (B.40), the first state of  $q(t)$  denoted by  $q(t)_1$  is a square wave with a period of  $2\pi/\omega$ . It shares the same phase as the reset triggered signal  $e_s(t)$  and has a magnitude of  $|E_n|\Delta_q^n(\omega)_1$ . Define a normalized square wave signal  $q_s(t)$  with the same phase as the reset-triggered signal  $e_s(t)$ , expressed as follows:

$$q_s(t) = \frac{4}{\pi} \sum_{\mu=1}^{\infty} \frac{\sin(\mu\omega t + \mu \angle E_s)}{\mu}, \mu = 2k + 1 (k \in \mathbb{N}), \quad (\text{B.41})$$

whose Fourier transform is given by

$$Q_s(\omega) = \mathcal{F}[q_s(t)] = 4 \sum_{\mu=1}^{\infty} \mathcal{F}[\sin(\mu\omega t + \mu \angle E_s)]/(\mu\pi). \quad (\text{B.42})$$

According to (B.37), (B.40) and (B.41),  $q(t)$  can be expressed as:

$$q(t) = |E_n|\Delta_q^n(\omega)q_s(t)/2 - |E_n|\Delta_v^n(\omega) + C_{\beta 2} + |E_n|\Delta_q^n(\omega)/2. \quad (\text{B.43})$$

For a time-domain signal  $q(t)$ , the frequency  $\omega$  is a constant. A constant function corresponds to a delta function in the frequency domain. Defining  $Q(\omega) = \mathcal{F}[q(t)]$ , we derive  $Q(\omega)$  from (B.43) as follows:

$$Q(\omega) = |E_n|\Delta_q^n(\omega)Q_s(\omega)/2 + (|E_n|\Delta_q^n(\omega)/2 - \Delta_v^n(\omega) + C_{\beta 2})\delta(\omega). \quad (\text{B.44})$$

Since  $\delta(\omega)$  is a Dirac delta function, which is zero for  $\omega \neq 0$ , equation (B.44) is simplified as:

$$Q(\omega) = |E_n|\Delta_q^n(\omega)Q_s(\omega)/2. \quad (\text{B.45})$$

From (B.42) and (B.45),  $Q(\omega)$  is given by

$$Q(\omega) = 2|E_n|\Delta_q^n(\omega) \sum_{\mu=1}^{\infty} \mathcal{F}[\sin(\mu\omega t + \mu\angle E_s)]/(\mu\pi). \quad (\text{B.46})$$

Both  $Q(\omega)$  (B.46) and  $Q_s(\omega)$  (B.42) contain  $\mu$  harmonics. Let  $Q^\mu(\omega)$  and  $Q_s^\mu(\omega)$  represent the  $\mu$ -th ( $\mu \in \mathbb{Z}^+$ ) harmonics of  $Q(\omega)$  and  $Q_s(\omega)$ , respectively. They are expressed as:

$$\begin{aligned} Q(\omega) &= \sum_{\mu=1}^{\infty} Q^\mu(\omega), \\ Q_s(\omega) &= \sum_{\mu=1}^{\infty} Q_s^\mu(\omega). \end{aligned} \quad (\text{B.47})$$

From (B.42), (B.46), and (B.47),  $Q_s^\mu(\omega)$  and  $Q^\mu(\omega)$  are given by

$$\begin{aligned} Q_s^\mu(\omega) &= 4\mathcal{F}[\sin(\mu\omega t + \mu\angle E_s)]/(\mu\pi), \\ Q^\mu(\omega) &= 2|E_n|\Delta_q^n(\omega)\mathcal{F}[\sin(\mu\omega t + \mu\angle E_s)]/(\mu\pi). \end{aligned} \quad (\text{B.48})$$

Let  $X_{nl}(\omega) = \mathcal{F}[x_{nl}(t)]$ , and  $X_{nl}^\mu(\omega)$  represents the  $\mu$ -th harmonic of  $X_{nl}(\omega)$ , defined as:

$$X_{nl}(\omega) = \sum_{\mu=1}^{\infty} X_{nl}^\mu(\omega). \quad (\text{B.49})$$

From (B.19), (B.48) and (B.49),  $X_{nl}^\mu(\omega)$  is derived as

$$X_{nl}^\mu(\omega) = (j\mu\omega I - A_R)^{-1} j\mu\omega I Q^\mu(\omega). \quad (\text{B.50})$$

According to (B.1), (B.49), and (B.50),  $X_c(\omega) = \mathcal{F}[x_c(t)]$  is obtained as

$$X_c(\omega) = X_{bl}(\omega) + \sum_{\mu=1}^{\infty} (j\mu\omega I - A_R)^{-1} j\mu\omega I Q^\mu(\omega), \quad (\text{B.51})$$

where  $X_{bl}(\omega) = \mathcal{F}[x_{bl}(t)]$ .

Let  $V(\omega) = \mathcal{F}[v(t)]$ . According to (1),  $V(\omega)$  is given by

$$V(\omega) = C_R X_c(\omega) + D_R E(\omega). \quad (\text{B.52})$$

Substituting  $X_c(\omega)$  from (B.51) into (B.52),  $V(\omega)$  is given by

$$V(\omega) = C_R X_{bl}(\omega) + D_R E(\omega) + \sum_{\mu=1}^{\infty} C_R (j\mu\omega I - A_R)^{-1} j\mu\omega I Q^\mu(\omega). \quad (\text{B.53})$$

From (1), we have

$$V_{bl}(\omega) = C_{bl}(\omega)E(\omega) = C_R X_{bl}(\omega) + D_R E(\omega). \quad (\text{B.54})$$

Then, substituting  $V_{bl}(\omega)$  from (B.54) into (B.53),  $V(\omega)$  is given by

$$V(\omega) = V_{bl}(\omega) + \sum_{\mu=1}^{\infty} C_R (j\mu\omega I - A_R)^{-1} j\mu\omega I Q^\mu(\omega). \quad (\text{B.55})$$

Define

$$\begin{aligned} V_{nl}(\omega) &= \sum_{\mu=1}^{\infty} V_q^\mu(\omega), \\ V_q^\mu(\omega) &= \Delta_x(\mu\omega) Q^\mu(\omega), \end{aligned} \quad (\text{B.56})$$

$$\Delta_x(\mu\omega) = C_R (j\mu\omega I - A_R)^{-1} j\mu\omega I \quad (\in \mathbb{R}^{1 \times n_c}).$$

and substitute  $V_q^\mu(\omega)$  from (B.56) into (B.55),  $V(\omega)$  is given by

$$V(\omega) = V_{bl}(\omega) + V_{nl}(\omega) = V_{bl}(\omega) + \sum_{\mu=1}^{\infty} V_q^\mu(\omega). \quad (\text{B.57})$$

In the time domain, equation (B.57) is given by

$$v(t) = v_{bl}(t) + v_{nl}(t). \quad (\text{B.58})$$

From (B.56),  $v_{nl}(t)$  is given by

$$v_{nl}(t) = \mathcal{F}^{-1} \left[ \sum_{\mu=1}^{\infty} \Delta_x(\mu\omega) Q^\mu(\omega) \right], \quad \mu \in \mathbb{Z}^+, \quad (\text{B.59})$$

where  $Q^\mu(\omega)$  and  $\Delta_x(\mu\omega)$  are defined in (B.56) and (B.48), respectively. Equations (B.58) and (B.59) conclude the proof.  $\square$

## Appendix C. Proof for Theorem 2

*Proof.* The reset controller  $C$ , operating with the input signal and reset-triggered signal  $e(t) = |E_1|\sin(\omega t + \angle E_1)$  at steady states is defined as the reset controller discussed in Theorem 1 when  $e_s(t) = e(t)$ .

Following a similar proof process as in Appendix Appendix B, consider that there are  $n \in \mathbb{N}$  harmonics in the reset output signal  $v(t)$ . Referring to (B.57), let  $V(\omega) = \sum_{n=1}^{\infty} V_n(\omega)$ , we obtain  $V_n(\omega)$  as

$$V_n(\omega) = \begin{cases} V_{bl}(\omega) + V_q^1(\omega), & \text{for } n = 1, \\ V_q^n(\omega), & \text{for odd } n > 1, \\ 0, & \text{for even } n \geq 2. \end{cases} \quad (\text{C.1})$$

By applying the ‘‘Virtual Harmonic Generator’’ Saikumar et al. (2021), the input signal  $e(t)$  generates  $n$  harmonics  $e_{1n}(t) = |E_1|\sin(n\omega t + n\angle E_1)$ , whose Fourier transform is  $E_{1n}(\omega) = |E_1|\mathcal{F}[\sin(n\omega t + n\angle E_1)]$ . From (B.56),  $C_{nl}(n\omega)$  is defined as

$$C_{nl}(n\omega) = \frac{V_q^n(\omega)}{E_{1n}(\omega)} = 2\Delta_x(n\omega)\Delta_q(\omega)/(n\pi). \quad (\text{C.2})$$

From (B.54), (C.1), and (C.2), the  $n$ -th HOSIDF for  $C$ , denoted as  $C_n(\omega)$ , is defined as

$$C_n(\omega) = \frac{V_n(\omega)}{E_{1n}(\omega)} = \begin{cases} C_{bl}(\omega) + C_{nl}(\omega), & \text{for } n = 1, \\ C_{nl}(n\omega), & \text{for odd } n > 1, \\ 0, & \text{for even } n \geq 2. \end{cases} \quad (\text{C.3})$$

This concludes the proof.  $\square$

#### Appendix D. Proof for Corollary 1

*Proof.* Define

$$V_{nl}(\omega) = \sum_{n=1}^{\infty} V_q^n(\omega). \quad (\text{D.1})$$

From (C.2), we have

$$V_q^n(\omega) = E_{1n}(\omega)C_{nl}(n\omega). \quad (\text{D.2})$$

From (D.1) and (D.2), the inverse Fourier transform of  $V_{nl}(\omega)$  is given by

$$v_{nl}(t) = \sum_{n=1}^{\infty} \mathcal{F}^{-1}[E_{1n}(\omega)C_{nl}(n\omega)]. \quad (\text{D.3})$$

From (B.57) and (D.1),  $V(\omega)$  given by

$$V(\omega) = V_{bl}(\omega) + V_{nl}(\omega). \quad (\text{D.4})$$

The inverse Fourier transform of  $V(\omega)$  is given in (25). This concludes the proof.  $\square$

#### Appendix E. Proof for Theorem 3

*Proof.* Consider a closed-loop reset control system (with reset controller  $C$  (1) where  $n_r = 1$ ), as depicted in Fig. 1 with a sinusoidal reference input signal  $r(t) = |R|\sin(\omega t)$  and under Assumptions 2 and 3, at steady states.

The Fourier transform of (32) is given by

$$\begin{aligned} V_l(\omega) &= \sum_{n=1}^{\infty} V_{bl}^n(\omega), \\ V_{nl}(\omega) &= \sum_{n=1}^{\infty} V_{nl}^n(\omega). \end{aligned} \quad (\text{E.1})$$

Based on (35) and (E.1), the signal  $v_l(t)$  in (33) is given by

$$v_l(t) = \sum_{n=1}^{\infty} \mathcal{F}^{-1}[E_n(\omega)C_{bl}(n\omega)]. \quad (\text{E.2})$$

The following section outlines the derivation of the signal  $v_{nl}(t)$  in (33). This process commences with the derivation of its first-order harmonic  $v_{nl}^1(t)$ . According to (25), the first  $C$  under an input signal and the reset-triggered signal of  $e_1(t) = |E_1|\sin(\omega t + \angle E_1)$ , yields the base-linear output denoted by  $v_{bl}^1(t)$  and the nonlinear output signal denoted by  $v_{nl}^1(t)$ . To generate the signal  $v_{nl}^1(t)$ , the ‘‘Virtual Harmonic Generator’’ is employed

to generate harmonics  $e_{1n}(t)$  from  $e_1(t)$ , as illustrated in Fig. 5(a), as given by:

$$e_{1n}(t) = |E_1|\sin(n\omega t + n\angle E_1), \quad n = 2k + 1 (k \in \mathbb{N}), \quad (\text{E.3})$$

whose Fourier transform is  $E_{1n}(\omega) = \mathcal{F}[e_{1n}(t)]$ .

The signal  $v_{bl}^1(t)$  is derived by (35). From (C.2), the signal  $v_{nl}^1(t)$  is given by:

$$v_{nl}^1(t) = \sum_{n=1}^{\infty} \mathcal{F}^{-1}[E_{1n}(\omega)C_{nl}(n\omega)]. \quad (\text{E.4})$$

In Fig. 5(a), consider a reset controller  $C$  with a sinusoidal input signal  $e_n(t) = |E_n|\sin(n\omega t + \angle E_n)$  and a reset triggered signal  $e_1(t) = |E_1|\sin(\omega t + \angle E_1)$ . From (34),  $V^n(\omega)$  is given by

$$V^n(\omega) = V_{bl}^n(\omega) + V_{nl}^n(\omega). \quad (\text{E.5})$$

From (21),  $V_{nl}^n(\omega)$  is given by

$$V_{nl}^n(\omega) = \sum_{\mu=1}^{\infty} \Delta_x(\mu\omega)Q^\mu(\omega), \quad (\text{E.6})$$

where  $\Delta_x(\mu\omega)$  and  $Q^\mu(\omega)$  are given in (22).

From (E.6),  $V_{nl}^n(\omega)$ , for a constant  $\omega$  and varying  $n$ , exhibit the same phase as the reset-triggered signal  $e_1(t)$ . Considering that  $V_{nl}^n(\omega)$  exhibits the same phase for different  $n$ , as indicated in (E.1), we introduce a function  $\Gamma(\omega)$  to express the ratio of  $V_{nl}(\omega)$  to  $V_{nl}^1(\omega)$ :

$$\Gamma(\omega) = \frac{V_{nl}(\omega)}{V_{nl}^1(\omega)} = \frac{\sum_{n=1}^{\infty} V_{nl}^n(\omega)}{V_{nl}^1(\omega)}. \quad (\text{E.7})$$

From (E.4) and (E.7),  $V_{nl}(\omega)$  is given by

$$V_{nl}(\omega) = \sum_{n=1}^{\infty} \Gamma(\omega)E_{1n}(\omega)C_{nl}(n\omega). \quad (\text{E.8})$$

From (E.1) and (E.8), we have

$$V_{nl}^n(\omega) = \Gamma(\omega)E_{1n}(\omega)C_{nl}(n\omega). \quad (\text{E.9})$$

Equations (33), (E.2), and (E.8) describe the new block diagram for the closed-loop RCS, presented in Fig. 5(b). In the new block diagram, the unknown parameter  $\Gamma(\omega)$  will be elucidated in the subsequent derivation.

By substituting  $V_{nl}^n(\omega)$  from (22) and (E.6) into (E.7),  $\Gamma(\omega)$  is simplified as

$$\Gamma(\omega) = \frac{\sum_{n=1}^{\infty} |E_n|\Delta_c^n(\omega)}{|E_1|\Delta_c^1(\omega)}. \quad (\text{E.10})$$

As illustrated in Fig. 5(b), in the closed-loop configuration, we have

$$E_n(\omega) = -V_n(\omega)C_\alpha(n\omega)\mathcal{P}(n\omega). \quad (\text{E.11})$$

Substituting (35) and (E.9) into (34),  $V_n(\omega)$  is given by

$$V_n(\omega) = E_n(\omega)C_{bl}(n\omega) + \Gamma(\omega)E_{1n}(\omega)C_{nl}(n\omega). \quad (\text{E.12})$$

Substituting (E.12) into (E.11), we have

$$E_n(\omega) = -E_n(\omega)\mathcal{L}_{bl}(n\omega) - \Gamma(\omega)E_{1n}(\omega)\mathcal{L}_{nl}(n\omega), \quad (\text{E.13})$$

where

$$\begin{aligned} \mathcal{L}_{bl}(n\omega) &= C_{bl}(n\omega)C_\alpha(n\omega)\mathcal{P}(n\omega), \\ \mathcal{L}_{nl}(n\omega) &= C_{nl}(n\omega)C_\alpha(n\omega)\mathcal{P}(n\omega). \end{aligned} \quad (\text{E.14})$$

Based on the definitions of  $e_n(t)$  and  $e_{1n}(t)$  provided in (13) and (E.3), we express (E.13) in the time domain as follows:

$$\begin{aligned} |E_n| |1 + \mathcal{L}_{bl}(n\omega)| \sin(n\omega t + \angle E_n + \angle(1 + \mathcal{L}_{bl}(n\omega))) = \\ - \Gamma(\omega) |E_1| |\mathcal{L}_{nl}(n\omega)| \sin(n\omega t + n\angle E_1 + \angle \mathcal{L}_{nl}(n\omega)). \end{aligned} \quad (\text{E.15})$$

From (E.15) and the given condition  $|E_n| > 0$ , we can deduce the following equations:

$$\begin{aligned} |E_n| &= \frac{\Gamma(\omega) |\mathcal{L}_{nl}(n\omega)|}{|1 + \mathcal{L}_{bl}(n\omega)|} |E_1|, \\ \angle E_n &= n\pi + n\angle E_1 + \angle \mathcal{L}_{nl}(n\omega) - \angle(1 + \mathcal{L}_{bl}(n\omega)), \\ &\quad \text{for } n = 2k + 1 > 1. \end{aligned} \quad (\text{E.16})$$

From (22),  $\Delta_c^n(\omega)$  is given by

$$\Delta_c^n(\omega) = |\Delta_l(n\omega)| \sin(\angle \Delta_l(n\omega) + \angle E_n - n\angle E_1). \quad (\text{E.17})$$

Substituting the relation between  $\angle E_1$  and  $\angle E_n$  ( $n > 1$ ) from (E.16) into (E.17), we obtain:

1. For  $n = 1$ ,

$$\Delta_c^1(\omega) = |\Delta_l(\omega)| \sin(\angle \Delta_l(\omega)). \quad (\text{E.18})$$

2. For  $n > 1$ ,

$$\Delta_c^n(\omega) = -|\Delta_l(n\omega)| \sin(\angle \Delta_l(n\omega) + \angle \mathcal{L}_{nl}(n\omega) - \angle(1 + \mathcal{L}_{bl}(n\omega))). \quad (\text{E.19})$$

Substituting  $\Delta_c^n(\omega)$  from (E.18) and (E.19) into (E.10), we have

$$\Gamma(\omega) = 1 + \frac{\sum_{n=3}^{\infty} |E_n| \Delta_c^n(\omega)}{|E_1| \Delta_c^1(\omega)}. \quad (\text{E.20})$$

Define

$$\Psi_n(\omega) = |\mathcal{L}_{nl}(n\omega)| / |1 + \mathcal{L}_{bl}(n\omega)| \quad (\text{E.21})$$

and substitute  $\Psi_n(\omega)$  from (E.21) into (E.16), we then obtain:

$$|E_n| = \Gamma(\omega) \Psi_n(\omega) |E_1|, \quad \text{for } n > 1. \quad (\text{E.22})$$

Substituting (E.21) and (E.22) into (E.20),  $\Gamma(\omega)$  is given by

$$\Gamma(\omega) = 1 + \Gamma(\omega) \frac{\sum_{n=3}^{\infty} \Psi_n(\omega) \Delta_c^n(\omega)}{\Delta_c^1(\omega)}. \quad (\text{E.23})$$

Derived from (E.23),  $\Gamma(\omega)$  is obtained as below:

$$\Gamma(\omega) = 1 / \left( 1 - \sum_{n=3}^{\infty} \Psi_n(\omega) \Delta_c^n(\omega) / \Delta_c^1(\omega) \right). \quad (\text{E.24})$$

Here,  $\Gamma(\omega)$  is derived and the proof of Theorem 3 is concluded.  $\square$

## Appendix F. Proof for Theorem 4

*Proof.* Consider a closed-loop SISO reset control system in Fig. 1 with a reset controller  $C$  (1) (where  $n_r = 1$ ) and to a sinusoidal reference input signal  $r(t) = |R| \sin(\omega t)$ , complying with Assumptions 2 and 3, at steady states.

From the block diagram for the closed-loop reset system in Fig. 5(b), we can express the first harmonic of the output  $Y(\omega)$  as  $Y_1(\omega)$ , given by

$$Y_1(\omega) = E_1(\omega) [\mathcal{L}_{bl}(\omega) + \Gamma(\omega) \mathcal{L}_{nl}(\omega)], \quad (\text{F.1})$$

where  $\mathcal{L}_{bl}(n\omega)$  and  $\mathcal{L}_{nl}(n\omega)$  are given in (E.14).

Let  $R_n(\omega) = |R| \mathcal{F}[\sin(n\omega t)]$ , in the closed loop, we have

$$Y_1(\omega) = R_1(\omega) - E_1(\omega). \quad (\text{F.2})$$

Combining (F.1) and (F.2), the first order sensitivity function for the closed-loop reset system, denoted as  $\mathcal{S}_1(\omega)$  is given by

$$\mathcal{S}_1(\omega) = \frac{E_1(\omega)}{R(\omega)} = \frac{1}{1 + \mathcal{L}_{bl}(\omega) + \Gamma(\omega) \mathcal{L}_{nl}(\omega)}. \quad (\text{F.3})$$

Define

$$\mathcal{L}_o(n\omega) = \mathcal{L}_{bl}(n\omega) + \Gamma(\omega) \mathcal{L}_{nl}(n\omega). \quad (\text{F.4})$$

Substituting (F.4) into (F.3),  $\mathcal{S}_1(\omega)$  is given by

$$\mathcal{S}_1(\omega) = \frac{1}{1 + \mathcal{L}_o(\omega)}. \quad (\text{F.5})$$

From (E.3) and (F.3), we obtain

$$E_{1n}(\omega) = |\mathcal{S}_1(\omega)| e^{jn\angle \mathcal{S}_1(\omega)} R_n(\omega), \quad (\text{F.6})$$

where  $R_n(\omega) = |R| \mathcal{F}[\sin(n\omega t)]$ .

Combining (E.13) and (F.6), the  $n$ -th ( $(n = 2k + 1, k \in \mathbb{N})$ ) sensitivity function for the closed-loop reset system, denoted by  $\mathcal{S}_n(\omega)$  is given by

$$\begin{aligned} \mathcal{S}_n(\omega) &= \frac{E_n(\omega)}{R_n(\omega)} = \frac{-\Gamma(\omega)\mathcal{L}_{nl}(n\omega) E_{1n}(\omega)}{1 + \mathcal{L}_{bl}(n\omega) R_n(\omega)} \\ &= -\frac{\Gamma(\omega)\mathcal{L}_{nl}(n\omega)|\mathcal{S}_1(\omega)|e^{jnL\mathcal{S}_1(\omega)}}{1 + \mathcal{L}_{bl}(n\omega)}. \end{aligned} \quad (\text{F.7})$$

According to Theorems 2 and 3, the even harmonics of  $\mathcal{S}_n(\omega)$  are zeros. The  $n^{\text{th}}$  complementary sensitivity function  $\mathcal{T}_n(\omega)$  in (39) and the control sensitivity function  $\mathcal{CS}_n(\omega)$  in (40) can be derived using the same method from (F.1) to (F.7). This concludes the proof.  $\square$

### CRedit authorship contribution statement

**Xinxin Zhang:** Conceptualization, Modelling & Simulation & Conducting Experiments & Analysis, Writing & editing. **Marcin B Kaczmarek:** Discussion & Review. **S. Hassan HosseinNia:** Conceptualization, Supervision, Review & editing.

### Declaration of competing interest

The authors declare that they have no known competing financial interests or personal relationships that could have appeared to influence the work reported in this paper.

### Declaration of Generative AI and AI-assisted technologies in the writing process

During the preparation of this work the authors used [ChatGPT] in order to improve readability and language. After using this tool, the authors reviewed and edited the content as needed and take full responsibility for the content of the publication.

### References

J. C. Clegg, A nonlinear integrator for servomechanisms, Transactions of the American Institute of Electrical Engineers, Part II: Applications and Industry 77 (1958) 41–42.  
L. Chen, N. Saikumar, S. Baldi, S. H. HosseinNia, Beyond the waterbed effect: Development of fractional order crone control with non-linear reset, in: 2018 annual american control conference (ACC), IEEE, 2018, pp. 545–552.  
K. Krishnan, I. Horowitz, Synthesis of a non-linear feedback system with significant plant-ignorance for prescribed system tolerances, International Journal of Control 19 (1974) 689–706.

I. Horowitz, P. Rosenbaum, Non-linear design for cost of feedback reduction in systems with large parameter uncertainty, International Journal of Control 21 (1975) 977–1001.  
L. Hazeleger, M. Heertjes, H. Nijmeijer, Second-order reset elements for stage control design, in: 2016 American Control Conference (ACC), IEEE, 2016, pp. 2643–2648.  
O. Beker, C. Hollot, Y. Chait, H. Han, Fundamental properties of reset control systems, Automatica 40 (2004) 905–915.  
A. Baños, A. Vidal, Definition and tuning of a PI+ CI reset controller, in: 2007 european control conference (ECC), IEEE, 2007, pp. 4792–4798.  
A. Baños, S. Dormido, A. Barreiro, Limit cycles analysis of reset control systems with reset band, Nonlinear analysis: hybrid systems 5 (2011) 163–173.  
N. Saikumar, H. HosseinNia, Generalized fractional order reset element (gfre), in: 9th European Nonlinear Dynamics Conference (ENOC), EUROMECH, 2017.  
C. Weise, K. Wulff, J. Reger, Fractional-order memory reset control for integer-order lti systems, in: 2019 IEEE 58th conference on decision and control (CDC), IEEE, 2019, pp. 5710–5715.  
C. Weise, K. Wulff, J. Reger, Extended fractional-order memory reset control for integer-order lti systems and experimental demonstration, IFAC-PapersOnLine 53 (2020) 7683–7690.  
N. Saikumar, R. K. Sinha, S. H. HosseinNia, “constant in gain lead in phase” element–application in precision motion control, IEEE/ASME Transactions on Mechatronics 24 (2019) 1176–1185.  
G. Tian, Z. Gao, Frequency response analysis of active disturbance rejection based control system, in: 2007 IEEE international conference on control applications, IEEE, 2007, pp. 1595–1599.  
S. Van Loon, K. Gruntjens, M. F. Heertjes, N. van de Wouw, W. Heemels, Frequency-domain tools for stability analysis of reset control systems, Automatica 82 (2017) 101–108.  
K. Ogata, Modern Control Engineering, Prentice Hall, Upper Saddle River, NJ, 2010.  
D. Deenen, M. F. Heertjes, W. Heemels, H. Nijmeijer, Hybrid integrator design for enhanced tracking in motion control, in: 2017 American Control Conference (ACC), IEEE, 2017, pp. 2863–2868.  
N. Saikumar, K. Heinen, S. H. HosseinNia, Loop-shaping for reset control systems: A higher-order sinusoidal-input describing functions approach, Control Engineering Practice 111 (2021) 104808.  
R. Beerens, A. Bisoffi, L. Zaccarian, H. Nijmeijer, M. Heemels, N. van de Wouw, Reset pid design for motion systems with stiction friction, IEEE Transactions on Control Systems Technology 30 (2021) 294–310.  
Y. Guo, Y. Wang, L. Xie, Frequency-domain properties of reset systems with application in hard-disk-drive systems, IEEE Transactions on Control Systems Technology 17 (2009) 1446–1453.  
A. A. Dastjerdi, A. Astolfi, N. Saikumar, N. Karbasizadeh, D. Valerio, S. H. HosseinNia, Closed-loop frequency analysis of reset control systems, IEEE Transactions on Automatic Control 68 (2022) 1146–1153.  
A. Banos, A. Barreiro, Reset control systems, Springer, 2012.  
Y. Guo, Y. Chen, Stability analysis of delayed reset systems with distributed state resetting, Nonlinear Analysis: Hybrid Systems 31 (2019) 265–274.  
A. Barreiro, A. Baños, S. Dormido, J. A. González-Prieto, Reset control systems with reset band: Well-posedness, limit cycles and stability analysis, Systems & Control Letters 63 (2014) 1–11.  
N. Karbasizadeh, N. Saikumar, S. H. HosseinNia, Fractional-order single state reset element, Nonlinear Dynamics 104 (2021) 413–427.  
A. Pavlov, N. Van De Wouw, H. Nijmeijer, Uniform output regulation of nonlinear systems: a convergent dynamics approach, volume 205, Springer, 2006.  
A. Pavlov, N. van de Wouw, H. Nijmeijer, Frequency response func-

- tions for nonlinear convergent systems, *IEEE Transactions on Automatic Control* 52 (2007) 1159–1165.
- K. Heinen, Frequency analysis of reset systems containing a clegg integrator: An introduction to higher order sinusoidal input describing functions (2018).
- J. Carrasco, A. Baños, A. Barreiro, Stability of reset control systems with inputs, in: 2008 16th Mediterranean Conference on Control and Automation, IEEE, 2008, pp. 1496–1501.
- E. Barabanov, A. Konyukh, Bohl exponents of linear differential systems, *Mem. Differential Equations Math. Phys* 24 (2001) 151–158.
- C. Hollot, O. Beker, Y. Chait, Q. Chen, On establishing classic performance measures for reset control systems, in: *Perspectives in robust control*, Springer, 2001, pp. 123–147.
- T. Samad, S. Mastellone, P. Goupil, A. van Delft, A. Serbezov, K. Brooks, Ifac industry committee update, initiative to increase industrial participation in the control community, *Newsletters April 2019. IFAC* (2019).
- P. Nuij, O. Bosgra, M. Steinbuch, Higher-order sinusoidal input describing functions for the analysis of non-linear systems with harmonic responses, *Mechanical Systems and Signal Processing* 20 (2006) 1883–1904.
- M. B. Kaczmarek, X. Zhang, S. H. HosseinNia, Steady-state non-linearity of open-loop reset systems, in: 2022 IEEE Conference on Control Technology and Applications (CCTA), IEEE, 2022, pp. 1056–1060.
- N. Karbasizadeh, A. A. Dastjerdi, N. Saikumar, S. H. HosseinNia, Band-passing nonlinearity in reset elements, *arXiv preprint arXiv:2009.06091* (2020).
- O. Beker, Analysis of reset control systems, University of Massachusetts Amherst, 2001.
- H. H. Pesaran, Y. Shin, Generalized impulse response analysis in linear multivariate models, *Economics letters* 58 (1998) 17–29.